Expanding and quantifying the crystal chemistry of the flexible ligand 15aneN5

Received 00th January 20xx,
Accepted 00th January 20xx

DOI: 10.1039/x0xx00000x

Anthony D. Shircliff,[a] Elisabeth M. A. Allbritton,[a] Dustin J. Davilla,[a] Michael-Joseph Gorbet,[a] Donald G. Jones,[a] David S. Tresp,[a] Michael B. Allen,[a] Alina Shrestha,[a] Gwendolyn E. Burgess,[a] John I. Eze,[a] Andrea T. Fernandez,[a] Daniel Ramirez,[a] Kody J. Shoff,[a] Garet G. Crispin,[a] Sarah B. Crone,[a] Michael Flinn,[a] Tien Tran,[a] Darby S. Bryce,[a] Abbagale L. Bond,[a] Dylan W. Shockey,[a] Allen G. Oliver,[c] Jeanette A. Krause,[d] Timothy J. Prior,*[b] and Timothy J. Hubin*[a]

Abstract: Tetraazamacrocycles have been very extensively exploited as transition metal ligands for a variety of purposes, including catalysis, medical imaging, pharmaceuticals, etc. However, the pentaazamacrocycles are much less commonly used for similar purposes because of poor availability, difficulties in their synthesis, and less well-known metal coordination properties. 1,4,7,10,13-pentaazacyclopentadane (**15aneN5**) was initially synthesized by a published synthetic route, which we simplified and shortened with minimal drop in yield. Eight different transition metal complexes were made using typical complexation methods. X-ray crystallography of multiple novel complexes yielded insight into the flexibility in coordination geometry of this interesting macrocycle as well as the first crystal structures of **15aneN5** with Cr^{3+}, Mn^{3+}, Fe^{3+}, Co^{3+}, Cu^{2+}, and Ru^{2+}. A parameter to quantify the coordination geometry adopted by the ligand was devised and applied to all known crystal structures of its metal complexes. Finally, oxidation of **15aneN5** to a novel diimine macrocycle was observed during complexation with ruthenium.

Introduction

A recent Google Scholar© search of the term "tetraazamacrocycl*" returned 2,420 references including that concept. A similar search for "pentaazamacrocycl*" returned just 92. While only a crude tool to highlight the ubiquity of the former over the scarcity of latter in the chemistry literature, it matches with our perception of the utilization of these ligand types based on our decades of experience as azamacrocycle chemists. Pentaazamacrocycles are pentadentate versions of the ubiquitous tetraazamacrocycles such as 1,4,8,11-tetraazacyclododecane (cyclam). Reasons for the underutilization of pentaazamacrocycles likely include their larger size, which is less suited to complexation of first-row transition metals; their odd-number of ring atoms, which is a well-known complication in the synthesis and utilization of otherwise analogous series; and the lack of synthetic approaches to their syntheses, which likely stems from both of these issues.

For tetraazamacrocycles, using cyclam as a common and relevant example, configurational analysis of the possible arrangements of the ligand around a transition metal ion has been aided by a substantial body of X-ray crystal structures and was laid out systematically by Bosnich, Poon, and Tobe over fifty years ago (Figure 1).[1]

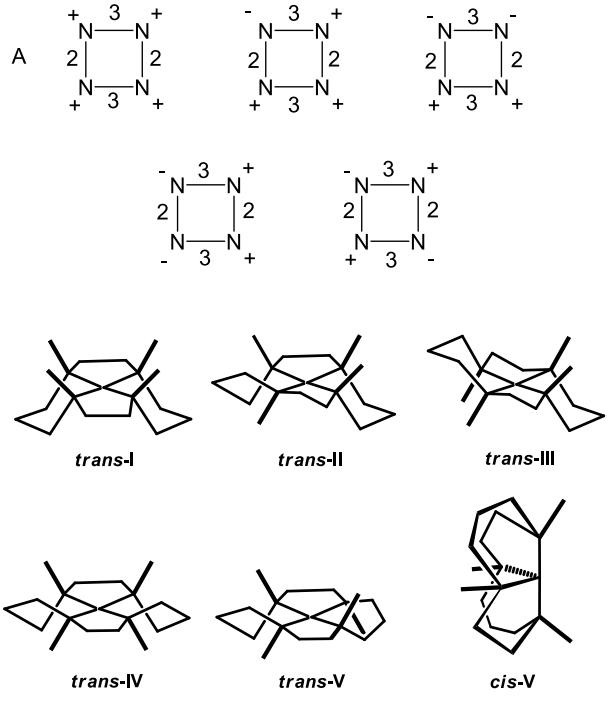

Figure 1. (A) Simple in-plane diagram for cyclam with hydrogen atoms attached to the four nitrogen atoms designated as above (+), or below (-) the plane. (B) A more sophisticated analysis based on 4- or 6-coordinate metal complexes where *cis* and *trans* describe potential monodentate ligand binding.

a Department of Chemistry and Physics, Southwestern Oklahoma State University, 100 Campus Drive, Weatherford, OK, USA E-mail: tim.hubin@swosu.edu http://faculty.swosu.edu/tim.hubin/
b Department of Chemistry, University of Hull, Cottingham Road, Kingston Upon Hull, HU6 7RX, UK
c Department of Chemistry and Biochemistry, University of Notre Dame, Notre Dame IN, USA
d Department of Chemistry, University of Cincinnati, Cincinnati, OH, USA

Electronic Supplementary Information (ESI) available: Data Tables and additional figures for X-ray crystal structures; metal complex characterization figures. See DOI: 10.1039/x0xx00000x

The combination of this analysis and the numerous crystal structure examples have allowed coordination chemists to study, predict, and even engineer the structural configuration of cyclam complexes in the solid state. Substitution of NH hydrogen atoms by alkyl and other functionalized pendant arms, including linked substituents (i.e. bridges) has allowed the confident planning of synthetic manipulations with a high likelihood that the desired outcomes will be realized, due to the vast database of known, structures.[2-7]

Much of our work has focused on ethylene *cross-bridged* tetraazamacrocycles over the last few decades. The cross-bridge rigidifies, and makes more topologically complex, the transition metal complexes of tetraazamacrocycles, while requiring the cis-V structure in Figure 1 above.[8-12] These are desirable traits for restricting the complex coordination geometry[13-18] and for applications where the kinetic stability of the complex is desirable, such as in biological or medical uses,[19-29] or in catalytic reactions under harsh conditions.[30-43] Recently, we have decided to investigate ethylene cross-bridged analogues of the larger pentaazamacrocycles, hoping to produce similarly useful, kinetically stable coordination complexes.[44] The most relevant conclusion from that work is that the glyoxal based ethylene cross-bridging synthetic strategy generally applied to tetraazamacrocycles is applicable to pentaazamacrocycles as well, and does induce the predicted kinetic stability. Revelations such as this suggest that the neglected pentaazamacrocycles should be further explored by coordination chemists. While that project is still ongoing, and will be further reported on separately, we have necessarily gained some insight into the synthesis of the parent pentaazamacrocycles themselves, which is the subject of this work.

Our initial target pentaazamacrocycle has been 1,4,7,10,13-pentaazacyclopentadecane, also known as **15aneN5** (Scheme 1). This compound is the simplest pentaaza analogue of omnipresent tetraazamacrocycles cyclam and cyclen and appeared to us as a logical beginning point for our studies. An analysis like that in Figure 1 for cyclam, although producing only four possible configurations in Figure 2A due to the ligand having only 2-carbon chains linking nitrogen atoms, unfortunately becomes complicated quickly (Figure 2B) due to the potential 5-, 6-, and 7-coordinate geometries available to **15aneN5** complexes, where only in the latter does *cis* and *trans* have meaning. A lack of published X-ray crystal structures (12 known prior to this work) meant we had only a very small database of structures to help guide us in prediction or engineering of solid state structures.

Here, we report our preparation of this pentaazamacrocycle in a significantly streamlined method, as well as our initial contributions to the expansion of its coordination chemistry and the available database of X-ray crystal structures to help in the development of an understanding of the coordination geometry adpted by this ligand. This pentaazamacrocycle has been reported previously in complexes with: first row transition metals Mn, Fe, Co, Ni, Cu, and Zn; second row transition metals Y, Ag and Cd; and Lanthanides La, Pr, Nd, Sm, Eu, Gd, Tb, Dy, Er, and Tm. However, a search of the Cambridge Structural Database revealed only 12 crystal structures containing metal complexes of this ligand, with only Fe^{2+}, Ni^{2+}, Zn^{2+}, Mn^{2+}, and La^{3+} represented. With the goal of widening the synthetic and structural knowledge of **15aneN5** transition metal complexes, we report below the synthesis, characterization, and X-ray crystal structures of additional Ni^{2+}, Fe^{2+}, and Zn^{2+} complexes, as well as the first crystal structures of this ligand with Cr^{3+}, Mn^{3+}, Fe^{3+}, Co^{3+}, Cu^{2+}, and Ru^{2+}. We observed certain patterns and limitations in the binding of **15aneN5** in its metal complexes and devised a structural factor that helps quantify the coordination geometry of this very flexible macrocycle.

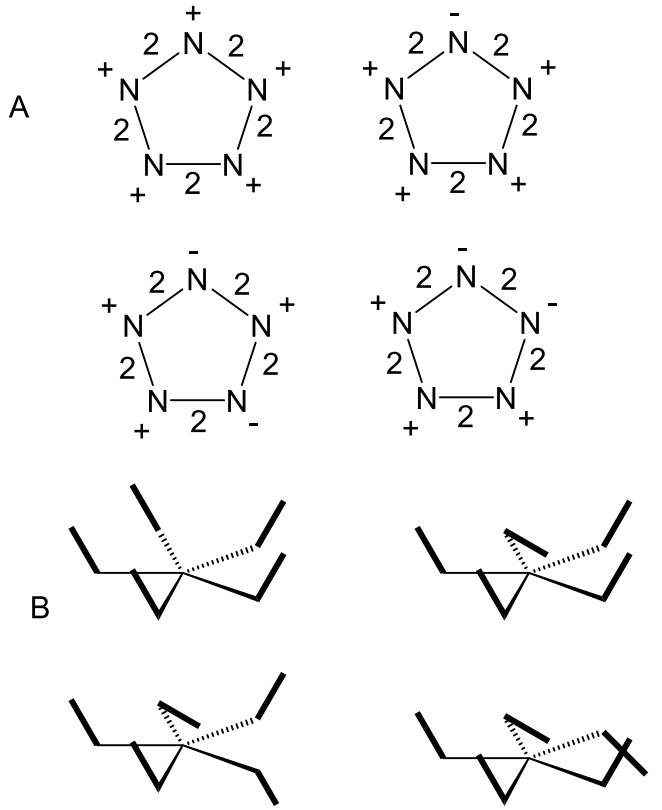

Figure 2. (A) Simple in-plane diagram for 15aneN5 with hydrogen atoms attached to the five nitrogen atoms designated as above (+), or below (-) the plane. (B) The beginnings of a more sophisticated analysis which was abandoned due to the potential 5-, 6-, and 7-coordinate geometries available to 15aneN5 complexes, where only in the latter does *cis* and *trans* have meaning.

Results and Discussion

Ligand Synthesis.

The original synthesis[45, 46] of **15aneN5** by Richman and Atkins combined 4-nitrogen and 1-nitrogen units, a strategy that was modified somewhat later.[47] More recently, a 3-nitrogen plus 2-nitrogen strategy was shown to be more convenient due to the commercial availability of the starting materials.[48] It is this synthesis, shown in Scheme 1, that we followed in our initial foray into pentaazamacrocyle chemistry.

As written,[48] this synthesis was successful in our hands, although never quite at the yields noted in the literature. But, due to several precautions against air and water, it is somewhat more difficult and lengthy than we found ideal. In addition, this synthesis was targeted for an undergraduate Inorganic Chemistry Laboratory course where complex glassware and long drying and extraction procedures would be limiting. Thus, we made several modifications to the synthetic procedure that included allowing water and air to be present at certain steps, as well as cutting down the overall preparation time by a number of days, with little loss in yield.

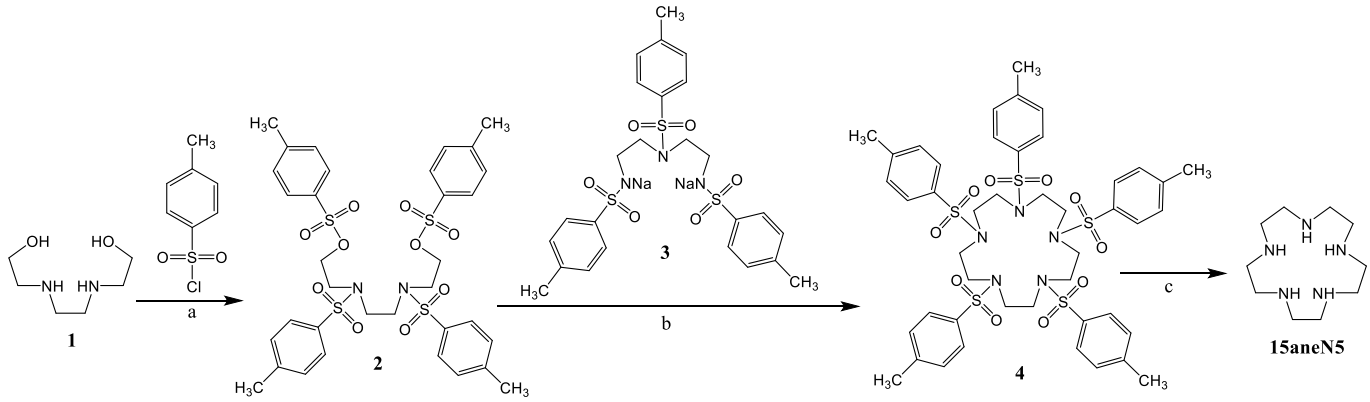

Scheme 1. Synthetic procedure for the production of **15aneN5**. a) CH_2Cl_2, NEt_3, 0 °C during 1 h addition, room temperature 12 h stirring, 73% Yield. b) DMF, 105 °C, 12 h, 43% Yield. c) i) H_2SO_4, 180 °C, 25 min. ii) Et_2O, filtration. iii) NaOH, H_2O, $CHCl_3$ extraction. 61% Yield.

In the first synthetic step, tetratosylation of *N*,*N*'-bis(2-hydroxyethyl)-ethylenediamine (**1**), little was changed in the reaction conditions. However, we were able to obtain the white solid product by filtration of the ethanol-washed solid open to the air on a glass frit, rather than under N_2 in a Schlenk filter. We also were able to obtain a dried product by simply drying the product under vacuum on its glass frit instead of drying it first under a stream of nitrogen. These modifications made this step more convenient and used less complex glassware and drying procedures. Our yields (on average 73%) were consistent with the literature procedure (81%).

The cyclization step was significantly shortened, primarily in the workup. The reaction itself was carried out similarly to the literature procedure.[48] This workup calls for drying the crude product obtained from precipitation with water to a constant mass in a vacuum oven. Then, a 5-day Soxhlet extraction with acetonitrile was used to separate the product from polymeric byproducts. We found that we could skip the drying step and avoid the 5-day Soxhlet extraction by simply using hot acetonitrile to extract the undried product directly through the glass frit upon which we had obtained the crude product. Polymeric byproducts remained on the frit and were discarded. Crystallization of the product from the acetonitrile/water solution obtained proceeded similarly to the literature procedure, although two crops could be obtained by successive reductions of solvent volume and cooling. The literature procedure cites a 64% yield, which we never approached whether we strictly followed the procedure, or followed our streamlined one. Our yields were generally somewhat lower, with 43% a representative yield. Again, these modifications made this step faster, more convenient, and used less complex and expensive glassware and drying procedures.

The final detosylation reaction was carried out similarly to the literature procedure, with only small changes to the workup, including filtration of the semisolid polyhydrosulfate salt open to air on a glass frit rather than under nitrogen and skipping the stream of nitrogen drying step. We never achieved the 85% yield noted in the literature procedure but averaged around 61% yield.

Overall, our changes to the synthetic procedure allowed a large scale, streamlined approach with less complex glassware, less protection from water and air, many days of drying and Soxhlet extraction bypassed, and somewhat lowered, but comparable yields in a process that was easily adapted for an undergraduate Advanced Inorganic Chemistry Laboratory course. Anecdotally, when attempts were made to purchase **15aneN5** from multiple commercial sources, the order was cancelled on more than one occasion as the company was unable to produce an acceptable amount or purity. When our procedure described above was transmitted to one of these companies and followed, 50g and 20g quantities were produced within weeks and at >97% purity.

Transition Metal Complexation.

Complexation of chloride and/or acetate salts of the respective metal ion generally occurred as expected by stirring with one equivalent of **15aneN5** in anhydrous MeOH in an inert atmosphere glovebox. In a few cases, DMF was used as the solvent if results from the MeOH reactions were not satisfactory. For methanol reactions, filtration removed trace solids, and then five equivalents of NH_4PF_6 were added to precipitate the respective PF_6^- salts. For the DMF reactions, solvent was removed and the residue redissolved in MeOH prior to precipitation.

There were a few notable observations regarding the syntheses or formulations of the complexes can be remarked on here. The Mn(**15aneN5**) complex has been formulated as the aqua complex, which is consistent with the elemental analysis. But the crystal structure clearly shows an NH_3 in the sixth coordination site. We believe that this may be a small impurity that happens to crystallize—NH_4PF_6 was used for precipitation of the PF_6^- salt and would provide a source of NH_3. Fe(**15aneN5**)Cl_2 was synthesized in DMF and did not precipitate with PF_6^-, suggesting both chlorides were bound giving a neutral complex. This was confirmed by the crystal structure (discussed below). [Fe(**15aneN5**)$(OAc)_2$](PF_6) showed signs of air oxidation when the Fe^{2+} complex was removed from the glovebox. So, Br_2 oxidation was carried out to prevent a mixture of air oxidized products and gave a clean oxidation to Fe^{3+}. Although synthetically not notable, [Co(**15aneN5**)Cl]Cl crystallized in three different forms, one containing no $CoCl_4^{2-}$, one a non-bound counterion $CoCl_4^{2-}$, and the final one a $CoCl_4^{2-}$ bound through a bridging chloride to the Co^{2+} metal ion.

Finally, the complexation of **15aneN5** with $RuCl_3 . xH_2O$ gave an oxidized diimine ligand designated **15aneN5-diimine** as shown in Scheme 2. The resulting metal complex, [Ru(**15aneN5-diimine**)Cl](PF_6), appears to be the result of a redox reaction where the Ru^{3+} reactant is converted to Ru^{2+} bound to the macrocycle, which has lost four hydrogen atoms and become a triamine/diimine pentaazamacrocycle with the imines adjacent to each other. The free ligand has been published once before as the product of a simple condensation reaction between the linear pentaamine and glyoxal.[49] No further literature references or metal complexes of this ligand are known. We will provide additional comparisons to similar ligand oxidations in tetraazmacrocyclic systems below as a case study of comparison between the tetraaza and pentaaza systems.

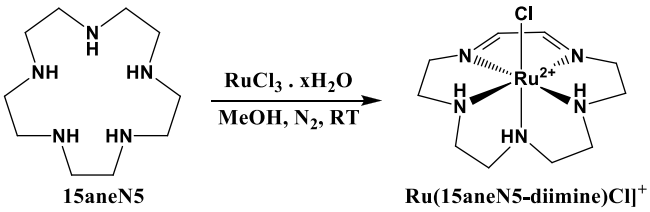

Scheme 2. Synthetic procedure for the synthesis of [Ru(**15aneN5-diimine**)Cl]$^+$

stacked in columns parallel to the crystallographic *a*-axis and between molecules within columns there are N-H···N hydrogen bonds.

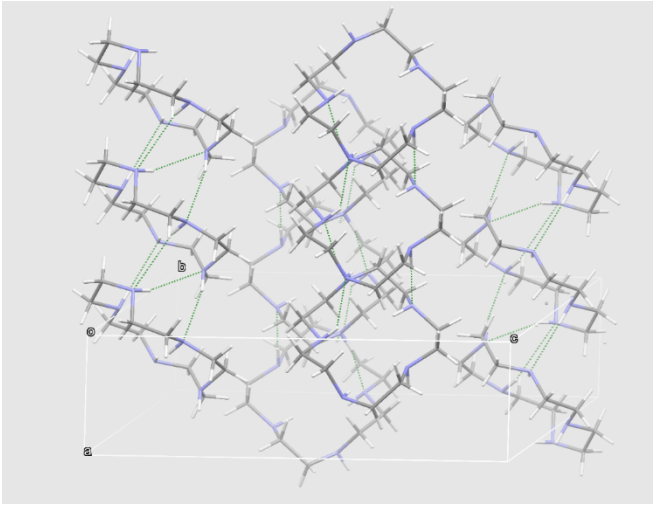

Figure 3: Representation of one molecule within the crystal structure of **15aneN5** with atoms shown as 50% probability ellipsoids (top). Solid state packing of ADS102, **15aneN5**. Dashed lines show classical hydrogen bonds (bottom).

Structural Studies

1) **15aneN5 ligand**

The synthetic route for **15aneN5** was confirmed using single crystal X-ray diffraction at intermediate stages; the crystal structures of compounds **2** and **3** have been determined. **2** crystallises in the centrosymmetric space group $P2_1/n$ with C-H···O interactions between adjacent molecules. The structure of **3** is also centrosymmetric (space group $P2_1/n$) but N-H···O hydrogen bonds assemble the molecules into tapes that run parallel to the crystallographic *a*-axis. There are further C-H···O interactions with and between the tapes. Full details of these structures are contained in the Supporting Information.

The crystal structures of the pure ligand **15aneN5** and the salt **$(15aneN5H_3)Cl_2(PF_6)$** have been determined. Details of the crystal structure of the salt are in the Supporting Information. The crystal structure of **15aneN5** has two independent molecules in the asymmetric unit; these are slightly different in the molecular conformation and one has very minor disorder. One molecule of the asymmetric unit is shown in Figure 3. These **15aneN5** molecules are

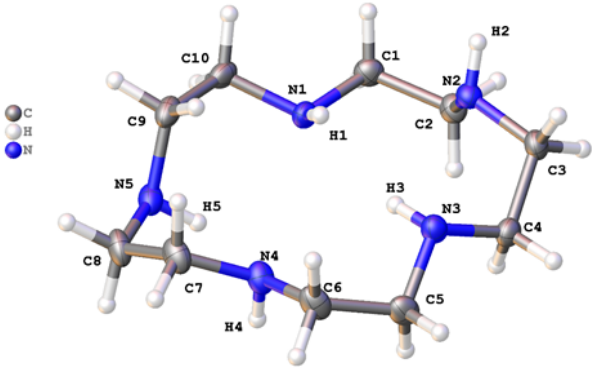

Transition metal ions fit inside the pocket of **15aneN5** and are coordinated by each of the nitrogen atoms. There are two principal orientations of the ligand observed in these complexes; the ligand can be in a roughly planar arrangement or it can twist so that four of the nitrogen atoms lie in a square plane and the fifth nitrogen is displaced above the plane. In these two extremes the coordination geometry about the metal ion by the five nitrogen atoms of the ligand is pentagonal planar or square pyramidal, as shown in Figure 4. We have classified geometry by using a factor, T, calculated as the square of the sine of the angle subtended by the distal M-N bond and the mean plane of the other four nitrogen atoms, shown as θ in Figure 4. Where the metal ion lies displaced from the mean plane of the nitrogen atoms this is taken into account in the calculations. For undistorted pentagonal planar geometry, T = 0, and for a regular square pyramid, T = 1. The use of the square of the sine of this angle returns a value of T = 0.5 when the angle is 45 ° but also helps to sharpen the change in the T value between the two extreme cases. For example, a complex that has one nitrogen 30 ° out of the plane of the others (but is essentially a distorted pentagonal planar geometry), T = 0.25.

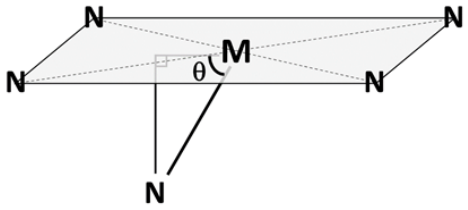

Figure 4: Idealised arrangement of five nitrogen ligand atoms around a metal ion in a distorted square pyramid.

2) **Seven coordinate complexes of 15aneN5**

The two iron complexes [Fe(**15aneN5**)$(CH_3COO)_2$](PF_6) and [Fe(**15aneN5**)Cl_2] each display 7-coordinate metal ions in which the nitrogen atoms of the **15aneN5** ligand are essentially in a plane and the coordination is completed above and below the plane by two further monodentate ligands. The two complexes are illustrated in Figure 5. The T values for these two complexes are 0.024 and 0.142 respectively. The complex [Fe(**15aneN5**)Cl_2] has a large spread of Fe-N bond lengths from 2.217(2) to 2.408(3) Å. The CSD reveals a similar structure, [Mn(**15aneN5**)Cl_2] (REFCODE PIHWEI),[50] that displays a very similar coordination geometry and orientation of the ligand with T = 0.168. The unit cell is similar to that of [Fe(**15aneN5**)Cl_2] but these are not isomorphous. The Mn-N bond lengths show similar variation to the analogous iron complex and lie in the range 2.262 to 2.445 Å. The Fe-N bond lengths in [Fe(**15aneN5**)$(CH_3COO)_2$](PF_6) are rather similar in length and lie in the range 2.245(3) to 2.286(5) Å. The Fe-O (axial) bond is shorter at 1.940(3)Å.

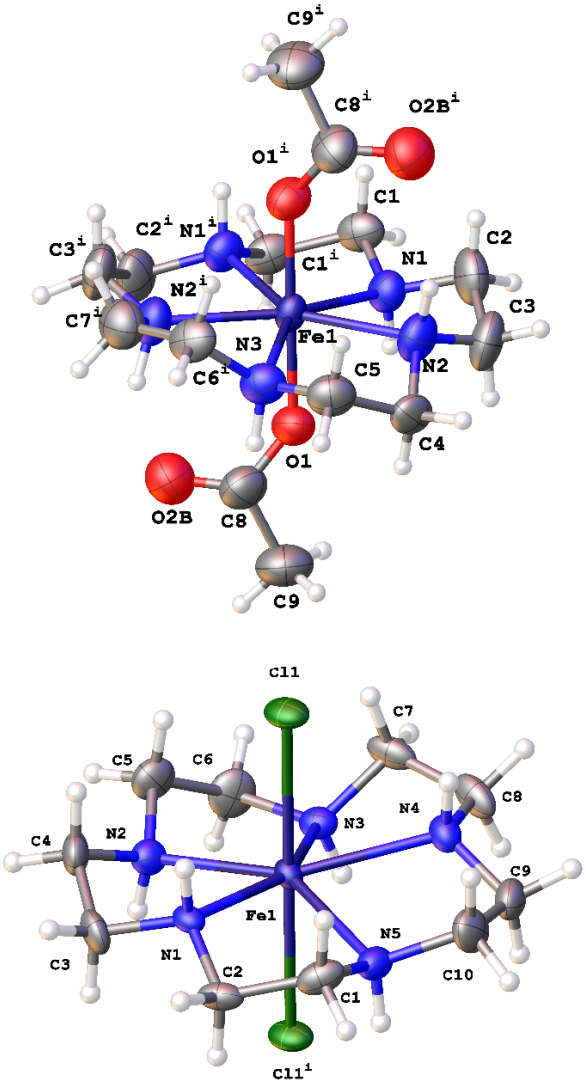

Figure 5: Complexes [Fe(**15aneN5**)$(CH_3COO)_2$](PF_6) (upper) and [Fe(**15aneN5**)Cl_2] (lower) with atoms drawn as 50% probability ellipsoids. Symmetry equivalent atoms are generated by i = ½-x, y, ½-z (left) and 1-x, -y, -z (right). Color scheme: iron deep blue, chloride green, carbon grey, hydrogen pale grey, nitrogen blue, oxygen red.

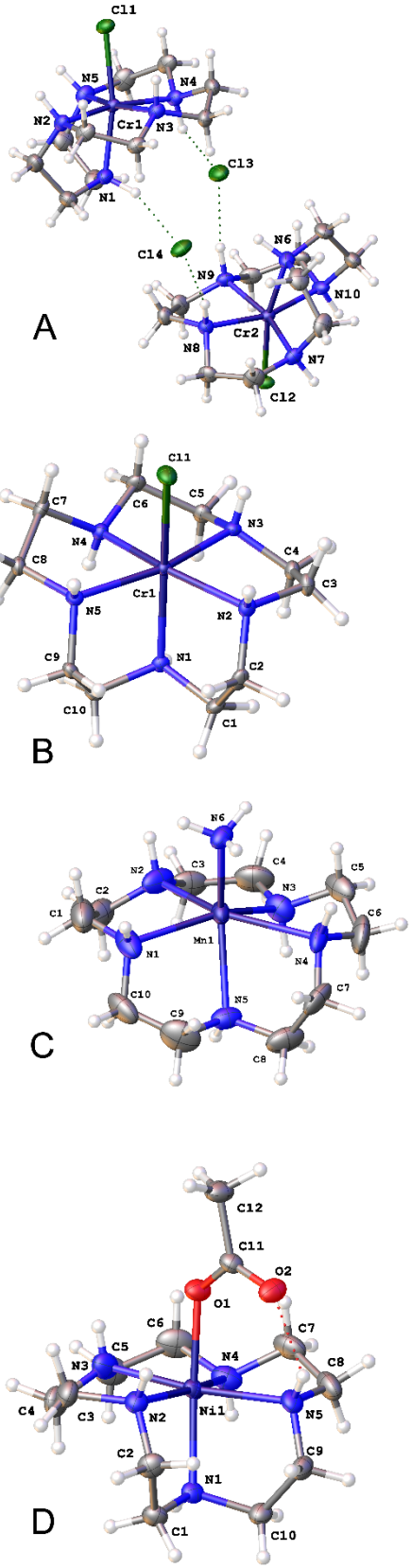

Figure 6: Metal centres in the complexes [Cr(**15aneN5**)Cl]Cl(PF6) (A), [Cr(**15aneN5**)Cl]$Cl_2(H_2O)$ (B), [Mn(**15aneN5**)NH_3]$(PF_6)_2$ (C), and [Ni(**15aneN5**)(CH_3COO)](PF_6) (D), with atoms drawn as 50% probability ellipsoids. Color scheme: metal deep blue, chloride green, carbon grey, hydrogen pale grey, nitrogen blue, oxygen red.

Table 1. Bond lengths at the metal centre for six coordinate complexes of **15aneN5** and **15aneN5**-diimine. In each case the axial nitrogen atom is starred and bolded.

Bond	Length (Å)	Bond	Length (Å)
[Cr(15aneN5)Cl]Cl(PF_6) T = 0.959 and T = 0.969			
Cr1–Cl1	2.3094(8)	Cr2–Cl2	2.3062(8)
Cr1–N1*	**2.114(2)**	**Cr2–N6***	**2.101(2)**
Cr1–N2	2.100(2)	Cr2–N7	2.097(2)
Cr1–N3	2.057(2)	Cr2–N8	2.043(2)
Cr1–N4	2.050(2)	Cr2–N9	2.035(2)
Cr1–N5	2.102(3)	Cr2–N10	2.091(2)
Cr(15aneN5)Cl]Cl_2(H_2O) T = 0.967			
Cr1–Cl1	2.3152(9)		
Cr1–N1*	**2.116(3)**		
Cr1–N2	2.099(3)		
Cr1–N3	2.039(3)		
Cr1–N4	2.058(3)		
Cr1–N5	2.103(3)		
[Mn(15aneN5)(NH_3)](PF_6)$_2$ T = 0.682 and T = 0.772			
Mn1–N1	2.370(13)	Mn1–N1A	2.204(12)
Mn1–N2	2.147(11)	Mn1–N2A	2.434(14)
Mn1–N3	2.184(12)	**Mn1–N3A***	**2.361(10)**
Mn1–N4	2.417(12)	Mn1–N4A	2.388(13)
Mn1–N5*	**2.361(10)**	Mn1–N5A	2.167(12)
Mn1-N6 (ammonia)	2.215 (3)		
[Co(15aneN5)]-μCl-[$CoCl_3$] T = 0.819			
Co1–Cl1	2.5690(8)		
Co1–N1*	**2.167(3)**		
Co1–N2	2.186(3)		
Co1–N3	2.153(3)		
Co1–N4	2.146(2)		
Co1–N5	2.186(2)		
[Co(15aneN5)Cl]$_2$[$CoCl_4$] T = 0.740			
Co1–Cl1	2.4376(5)		
Co1–N1*	**2.2080(16)**		
Co1–N2	2.2213(16)		
Co1–N3	2.1749(15)		
Co1–N4	2.1502(16)		
Co1–N5	2.2406(16)		
[Co(15aneN5)Cl]Cl T = 0.781 and T = 0.923			
Co1–Cl1	2.4700(10)	Co2–Cl2	2.5074(11)
Co1–N1	2.182(3)	**Co2–N6***	**2.179(3)**
Co1–N2	2.193(3)	Co2–N7	2.149(3)
Co1–N3*	**2.137(3)**	Co2–N8	2.135(3)
Co1–N4	2.160(3)	Co2–N9, Co2–N9A	2.168(6), 2.160(6)
Co1–N5	2.162(3)	Co2–N10	2.140(3)
[Ni(15aneN5)(CH_3COO)](PF_6) T = 0.943			
Ni1–O1	2.0859(16)		
Ni1–N1*	**2.1490(19)**		
Ni1–N2	2.119(2)		
Ni1–N3	2.073(2)		
Ni1–N4	2.089(2)		
Ni1–N5	2.094(2)		
[Ru(15aneN5-diimine)Cl](PF_6) T = 0.922			
Ru1–Cl1	2.3945(5)		
Ru1–N1	2.1763(16)		
Ru1–N2 (imine)	1.9508(16)		
Ru1–N3 (imine)	1.9414(17)		
Ru1–N4	2.1511(17)		
Ru1–N5*	**2.0987(16)**		

3) **Six coordinate complexes of 15aneN5**

The majority of other complexes in this study have 6-coordinate metal ions and there is a pronounced tendency towards square pyramidal coordination by the five nitrogen atoms of the ligand, but there is variation in the position of the fifth nitrogen atom relative to the others. In particular, Cr^{3+} and Ni^{2+} show coordination environments near to an undistorted square pyramid, as might be expected on ligand field grounds. Table 1 lists bond lengths around the metal ion for all 6-coordinate structures.

[Cr(**15aneN5**)Cl]Cl_2(H_2O) and [Cr(**15aneN5**)Cl]Cl(PF_6) each display Cr^{3+} in a 6-coordinate environment composed of five nitrogen atoms and one chloride that is close to being a regular octahedron. (Figure 6A and 6B). For [Cr(**15aneN5**)Cl]Cl_2(H_2O) the value of T is 0.967. For [Cr(**15aneN5**)Cl]Cl(PF_6) there are two symmetry-independent complexes in the asymmetric unit and these have T values of 0.959 and 0.969. The bond lengths around the chromium ion for each of these structures are given in Table 1. There is limited variation in the Cr–N distances, but is notable in each case that the *axial* nitrogen atom is a little further away from the metal than the other ligating nitrogen atoms. These are the first examples of chromium complexes with the **15aneN5** ligand.

[Mn(**15aneN5**)NH_3](PF_6)$_2$ displays 6-coordinate Mn (Figure 6C) but there is a distortion away from a regular octahedral coordination and T = 0.682 and 0.772 (the two values corresponds to two orientations of the ligand found in the solid state.) The Mn-N bond lengths shown in Table 1 display considerable variation; there are two short Mn-N bonds of around 2.18 Å and three longer ones nearer 2.4 Å.

The CSD contains another example of a similar Mn complex (REFCODE NAYSEI),[51] [Mn(**15aneN5**)NO_3](NO_3), and this displays rather similar coordination about the Mn^{2+} ion. The coordination here is rather well described as a distorted trigonal prism and this is reinforced by the Mn-N bond lengths which lie in the range 2.273 to 2.308 Å (mean 2.283 Å, σ = 0.013 Å).

There is a further Mn example (REFCODE OSUZOT)[52] that features Mn in both 6- and 7- coordinate environments. The 7-coordinate Mn centres are linked by $[Mo(CN)_6]^{3-}$ ions to form a coordination polymer. This is decorated by one [Mn(**15aneN5**)] complex at each Mo centre. There is considerable disorder present in the structure and multiple orientations of the ligand around the Mn ions generated by symmetry. The 7 coordinate centre has the ligand in a close to planar arrangement with T = 0.04. For the 6-coordinate case, the ligand is in a rather distorted square planar arrangement with T = 0.806.

The cobalt compounds [Co(**15aneN5**)Cl]Cl, [Co(**15aneN5**)Cl]$_2$[$CoCl_4$], and [Co(**15aneN5**)]-μCl-[$CoCl_3$] each feature the distorted octahedral ion $[Co(\mathbf{15aneN5})Cl]^{2+}$ and are the first examples of cobalt complexes of this ligand. The three complexes are illustrated in Figure 7. The first two have discrete cationic complexes but in the third the anionic unit $[CoCl_4]^{2-}$ is coordinated to the $[Co(\mathbf{15aneN5})]^{2+}$ unit through one of the chlorides. In [Co(**15aneN5**)Cl]Cl there are two symmetry-independent metal complexes which have somewhat different geometries; for the two different Co ions, the T values are 0.781 and 0.923. For [Co(**15aneN5**)Cl]$_2$[$CoCl_4$] there is a single cationic complex in the asymmetric unit and this has T = 0.740. The $[CoCl_4]^{2-}$ ion in these two complexes is a regular tetrahedron. In [Co(**15aneN5**)]-μCl-[$CoCl_3$] the T value is 0.819. [Co(**15aneN5**)Cl]$_2$[$CoCl_4$], and [Co(**15aneN5**)]-μCl-[$CoCl_3$] each have a very narrow range of Co-N bond lengths (Table 1). It is notable that the bridging chloride is much further from the metal ion than the monodentate chloride. The Co-N bond lengths in [Co(**15aneN5**)Cl]$_2$[$CoCl_4$] show much greater variation with the range of values being 2.1502(16) to 2.2406(16) Å.

It is notable that the Co-N bond of the axial nitrogen is the longest (2.2080(16)Å).

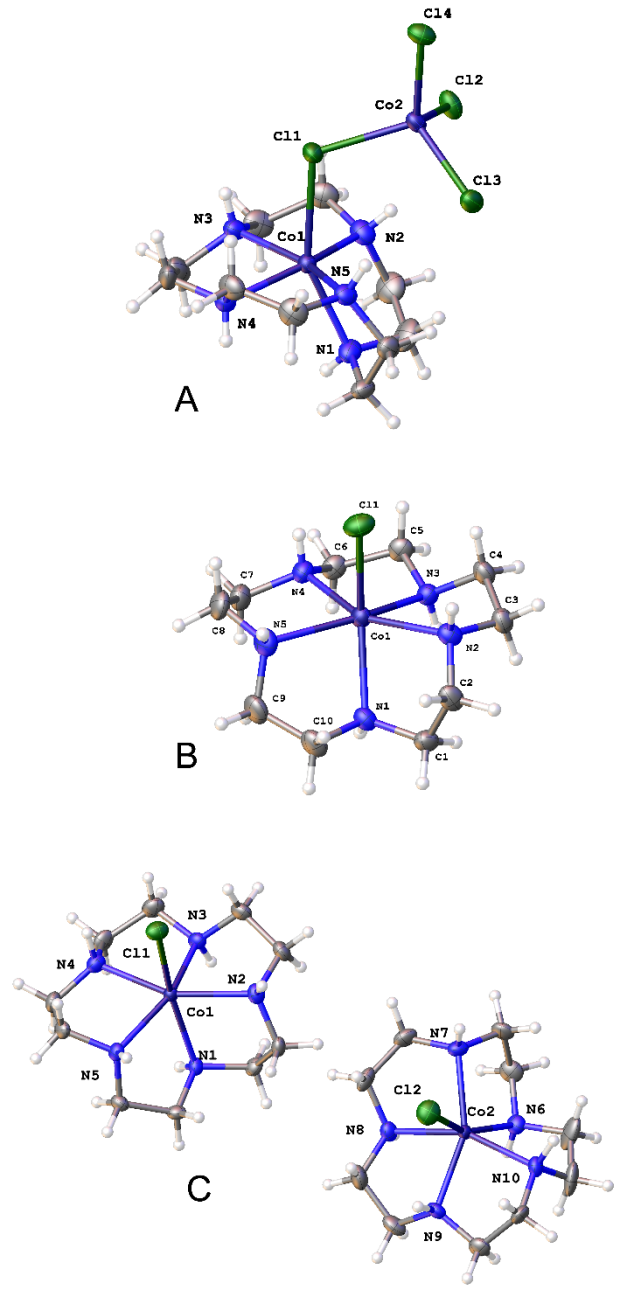

Figure 7: Metal centres in the complexes [Co(**15aneN5**)]-µCl-[$CoCl_3$] (A), [Co(**15aneN5**)Cl]$_2$[$CoCl_4$], (B), and [Co(**15aneN5**)Cl]Cl (C), with atoms drawn as 50% probability ellipsoids. Colour scheme: cobalt deep blue, chloride green, carbon grey, hydrogen pale grey, nitrogen blue.

The Ni^{2+} complex [Ni(**15aneN5**)(CH_3COO)](PF_6) is also 6-coordinate and features a slightly distorted octahedral coordination geometry (T = 0.943) and monodentate acetate (Figure 6D). The Ni-N bonds of the ligand within the square plane are somewhat shorter than the Ni-N bond to the axial nitrogen (2.1490(19) Å) which is the longest bond. The acetate is strictly monodentate (Ni-O 2.0859(16) Å) and bond lengths of the carboxylate are 1.270(3) and 1.249(3) Å (O-C-O bond angle is 124.7(2) °). The unbound carbonyl acts as a hydrogen bond acceptor; it forms an intramolecular hydrogen bond with N5-H5 (O12···N5 is 2.837(3)Å) and an intermolecular hydrogen bond with N1^{i}-H1^{i} (O12···N1i is 2.882(2) Å, i = 1.5–x, 1–y, z–0.5). These two interactions lead to the formation of a hydrogen-bonded chain that runs parallel to the crystallographic c-axis. Between chains are located PF_6 anions and these form C-H···F contacts.

There have been several other nickel complexes of **15aneN5** reported and these each display slightly-distorted octahedral coordination about the metal. [Ni(**15aneN5**)(OH_2)](ClO_4)(NO_3) (REFCODE JISTEK)[53] has an almost regular square pyramidal arrangement of the macrocyclic ligand and a T value 0.983.

The complexes [M($CN)_3${µ-CN-Ni(**15aneN5**)}$^{54}_3$]$^{3+}$ (M Cr, Fe)[55] have been reported as their perchlorate salts (CSD REFCODES XOCXAP and XOCXET).[55, 56] The Ni^{2+} ions in these are surrounded by six nitrogen atoms in approximately octahedral coordination at the Ni^{2+} ion (T = 0.932 and 0.924 for the Cr and Fe complexes respectively). In each of these four Ni^{2+} examples, the Ni-N bond of the axial nitrogen is the longest bond at the coordination centre.[47]

The six coordinate complex [Ni(**15aneN5**)(ClO_4)](ClO_4) (REFCODE HABKOK)[57] shows similar geometry to the others above and is slightly distorted octahedral geometry (T = 0.931). The Ni-O bond to perchlorate is rather long (2.345 Å) in line with other similar complexes. The shortest Ni-N bond is the axial nitrogen that is trans to this ligand in contrast to the other examples above.

4) **Five coordinate complexes of 15aneN5**

The copper and zinc complexes [Cu(**15aneN5**)](PF_6) . 2(CH_3NO_2) and [Zn(**15aneN5**)](PF_6)$_2$ each contain 5-coordinate metal ions. (Figure 8) [Cu(**15aneN5**)](PF_6)$_2$. 2(CH_3NO_2) crystallises in the non-centric space group $P2_1$ with a single copper ion in the asymmetric unit. There are four short Cu-N bonds in an approximately square plane (bond lengths 2.0067(3) to 2.063(2) Å) and one longer bond that lies out off the plane (Cu-N1 distance is 2.1770(19) Å). This 5-coordinate geometry with one long bond is common for copper and is consistent with the presence of a Jahn-Teller distortion. The T value for this complex is 0.821 and the geometry index τ_5 is 0.067, both of which confirm a somewhat distorted square planar geometry at the metal.[58]

The Zn-N bond lengths in [Zn(**15aneN5**)](PF_6)$_2$ display a rather large range, from 2.054(4) to 2.158(4) Å with the shortest being for N5, the distal nitrogen atom. It is possible to identify the geometry of the ligand using T, which is 0.768 here, showing a distorted square planar arrangement of the nitrogen atoms. The geometry index τ_5 is 0.25 confirming this is a distorted square planar complex rather than being trigonal bipyramidal.

There is one previous example of a five coordinate complex of Zn^{2+}, namely [Zn(**15aneN5**)](ClO_4)$_2$ (T = 0.790). The coordination is very similar to that in the present case.[59] The other known complexes, [Zn(**15aneN5**)SCH_2Ph](ClO_4) and [Zn(**15aneN5**)S-pTol](ClO_4), are six coordinate. (REFCODE ICUGOD, T = 0.863 and REFCODE ICUGUJ, T = 0.824, 0.828).[59]

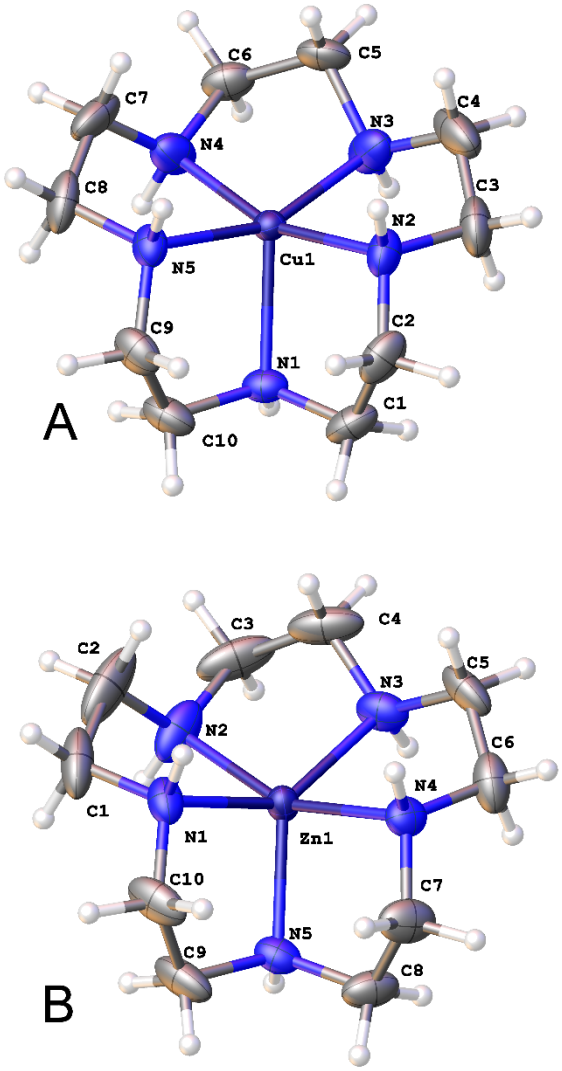

Figure 8: Metal centres in the complexes [Cu(**15aneN5**)]$(PF_6)_2$. $2(CH_3NO_2)$ (A) and [Zn(15aneN5)]$(PF_6)_2$ (B) with atoms drawn as 50% probability ellipsoids. Colour scheme: metal deep blue, carbon grey, hydrogen pale grey, nitrogen blue.

5) **Additional 15aneN5 structures**

Although we have not focused on lanthanide complexes in this study, there is one further structure in the CSD of **15aneN5** and this is an 11-coordinate La^{3+} structure (REFCODE NOVKEO)[55] containing the ion [La(**15aneN5**)$(NO_3)_3$] in which each nitrate is bidentate. The **15aneN5** is neither in a planar arrange or square pyramid, but has bent towards an inverted V-shape so that the five nitrogen atoms are all projecting upwards towards the La^{3+} with the ethylene links downwards.

From the examples here it appears that **15aneN5** cannot quite adopt a perfectly regular square-based pyramidal geometry about a metal as the macrocycle is too strained for the fifth nitrogen to wrap round and become perfectly axial to the plane of the other four nitrogen atoms. Elongation of two of the ethylene bridges in **15aneN5** could lead to less-strained square-based pyramidal coordination at a metal centre. There is a single example of this ligand (L = 1,4,7,10,14-penta-azacycloheptadecane-N,N',N'',N''',N'''') in the CSD (REFCODE FOHGUE)[47] and it features the 6-coordinate ion $[CoLCl]^{2+}$ in which the ligand adopts a very regular square pyramidal arrangement with T = 0.958 and the N-Co-Cl (trans) angle is 175.4 °. It is notable that the C_3H_6 links do not join to the axial nitrogen, but these join nitrogen atoms within the square plane. Presumably, this arrangement allows the twisting of the ligand to facilitate a strictly axial position for the fifth nitrogen. The position of the axial nitrogen atom (and M–N bond length) seems to depend strongly on the ligands trans to it. Where the axial nitrogen is trans to a good ligand such as cyanide, this is a rather long bond, but when it is trans to a poor ligand (such as perchlorate) this bond is much shorter.

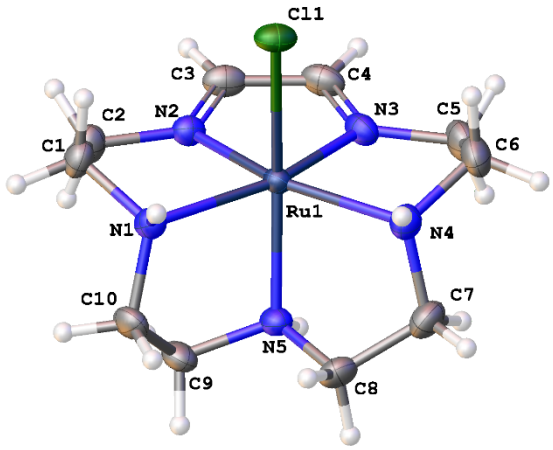

Figure 9: Metal centre in [Ru(**15aneN5**-diimine)Cl](PF_6) with atoms drawn as 50% probability ellipsoids. Colour scheme: ruthenium deep blue, chloride green, carbon grey, hydrogen pale grey, nitrogen blue.

A Case Study for Tetraaza-Pentaaza Comparison: Ruthenium-Imine Chemistry

1) **The [Ru(15aneN5-diimine)Cl](PF$_6$) structure**

The final 6-coordinate structure in this study features the 4d metal Ru. As discussed above, the ligand has reacted in the preparation of the metal complex and has been oxidised so that two adjacent secondary amines have been converted into imines. The reaction yields a crystalline product with formula [Ru(**15aneN5-diimine**)Cl](PF_6) containing 6-coordinate Ru^{2+} in a distorted octahedral environment (Figure 9). The adjacent pair of nitrogen atoms from the two imines (N2 and N3) form short Ru-N bonds (1.9508(16) and 1.9414(17) Å) and a bite angle of 80.02(7)°. In the plane, the other two Ru-N bonds are longer (2.1763(16) and 2.1511(17) Å) and of a similar length to the one that is almost orthogonal to this plane (2.0987(16) Å). The fifth nitrogen atom is almost orthogonal to the plane of the four nitrogen atoms with T = 0.922.

There are five Ru-cyclen crystal structures in the Cambridge Structural Database. Three of these are for 'capsule' molecules and have poorly ordered guests. The remaining two are both discrete metal complexes with cyclen bound in cis-V shape. We have chosen the one closest to our systems for comparison, [Ru(bipy)(cylclen)]Cl_2, CCDC REFCODE WEMFUQ.[60] In this, the cyclen is not planar but adopts a taco shape with N2 and N4 at the apex of the taco and N1 and N3 at the top of each side. (See Figure 10) The geometries at N1 and N3 are very similar, and these are different from the geometries at N2 and N4 which themselves are very similar. The Ru1 to N1 and N3 bonds are 2.103 and 2.104 Å while those to N2 and N4 are a little

longer at 2.130 and 2.117 Å respectively (unfortunately there are no esu values given in the original paper). These distances are all much longer than the Ru to imine distances in [Ru(15aneN5-diimine)Cl](PF$_6$) but shorter than the in place Ru–N distance and similar to the axial Ru–N. The C–N distances in [Ru(bipy)(cylclen)]Cl$_2$ for N1 and N3 lie in clustered around 1.470 Å and for N2 and N4 the value is longer around 1.497 Å. These C–N single bonds are similar in length to those in the bound 15aneN5-diimine. C–N–C angles in both compounds for are similar. It is notable in each cyclic ligand that there is substantial variation in bond lengths upon binding of Ru^{2+} as a direct result of the ligand geometry. The geometric parameters of the complexes [Ru(bipy)(cylclen)]Cl$_2$ and [Ru(15aneN5-diimine)Cl](PF$_6$) are entirely consistent and a confirmation of the presence of the diimine.

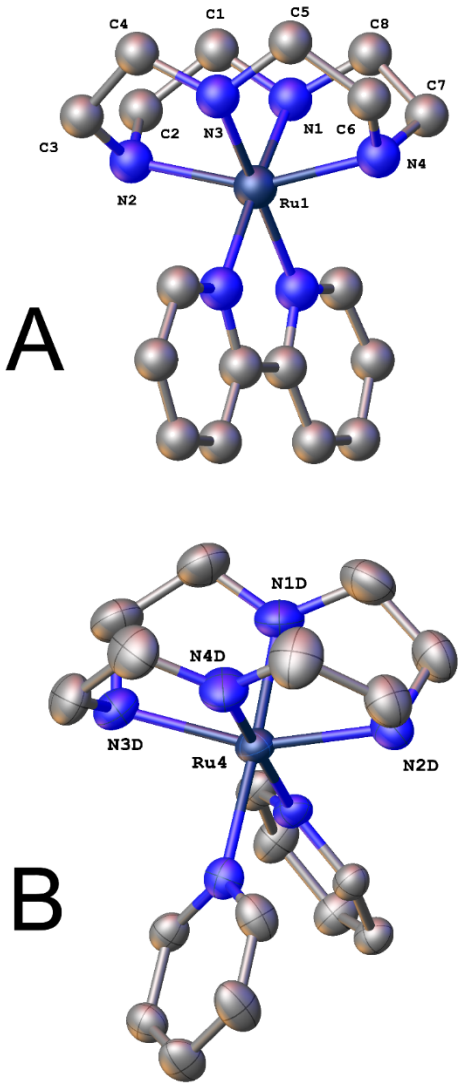

Figure 10: Coordination about Ru^{2+} in WEBFUQ (A)[60] and RIFTAD (B).[61] Note the taco shape adopted by the cyclen ligand in each case.

There is a similar report of the oxidation of a cyclen by Ru^{3+} to generate a macrocycle featuring C–N and C=N bonds in the capsule ion $[(tpt)_4(RuL)_6]^{12+}$ where tpt = tris(3-pyridyl)triazine and L is the partly oxidised cyclen ligand with one imine, with CCDC REFCODE RIFTAB.[61] The crystallography of this compound is complicated by the fact that the asymmetric unit is large and comprises the whole capsule containing six Ru^{2+} ions. However, it is possible to compare the geometry at the Ru in this compound with that in [Ru(15aneN5-diimine)Cl](PF$_6$). The coordination geometry about the six independent Ru^{2+} ions is reasonably consistent and mean values for the bond lengths have small standard deviations, so these are used for comparison. One example Ru centre is illustrated in Figure 10. Some observations are immediately obvious: (1) imine Ru–N bond lengths in [Ru(15aneN5-diimine)Cl](PF6) (1.9508(16) and 1.9414(17) Å) are shorter than those identified in $[(tpt)_4(RuL)_6]^{12+}$ (2.023 Å); (2) amine Ru–N bond lengths are similar at around 2.15 Å; (3) C=N bonds in [Ru(15aneN5-diimine)Cl](PF6) (1.313(3) and 1.317(3)Å) are somewhat shorter than typical equivalent bonds in $[(tpt)_4(RuL)_6]^{12+}$ which are around 1.35 Å; (4) the bond angles at the imine nitrogen (125.36(18) and 125.54(18)° in [Ru(15aneN5-diimine)Cl](PF$_6$)) are similar in both compounds (124 ° in $[(tpt)_4(RuL)_6]^{12+}$).

However, while our X-ray diffraction data clearly shown that a vicinal diimine has formed in the reaction, the picture is not so clear for $[(tpt)_4(RuL)_6]^{12+}$ and there is evidence that the simple model employed of a single imine in the same position in each oxidised cyclen is incomplete. Of the four nitrogen atoms, bond angles at two of them (N2D, N3D etc) are close to 113 °, but for the other two (N1D, N4D etc), the mean bond angles are 122 and 124 ° implying that these are not amines. Similarly, the C–N bond lengths are intriguing; two nitrogens with bond angles 113 ° have pairs of C–N very closely clustered on 1.50 Å, but for the other two nitrogens (bond angles 122, 124°) the mean values are 1.35 & 1.43 Å and 1.395 & 1.435 Å. One possible explanation is that there is really a second imine present in each of these "N4" macrocycles. More likely is that the location of the imine is disordered through the structure and this disorder has not yet been modelled. Figure S12b in the supplementary information shows the bond lengths and angles at each nitrogen atoms in the three Ru structure discussed here.[60, 61]

2) **Ruthenium and Amine Oxidation to Imines**

The diimine Ru^{2+} structure appears to be the first example of pentaazamacrocycle ligand oxidation to an imine by its coordinated metal ion. However, the phenomenon of transition metals oxidizing their complexed macrocyclic amines to imines is well known, as revealed by Busch for nickel and iron complexes.[62-64] Similar Ru complex chemistry is known in bidentate amine chelates,[65, 66] and tetraazamacrocycles,[67] dating back at least to the 1970's. Taube invokes the stabilization of Ru^{2+} by π-back donation to the imine as the driving force for imine formation.[66] Ru^{3+} imine complexes are notably less stable than their Ru^{2+} couterparts,[66] due to the increased Lewis acidity of the former. According to Taube's accepted mechanism for the amine to imine oxidation,[66] the two-step process is shown in Scheme 3.

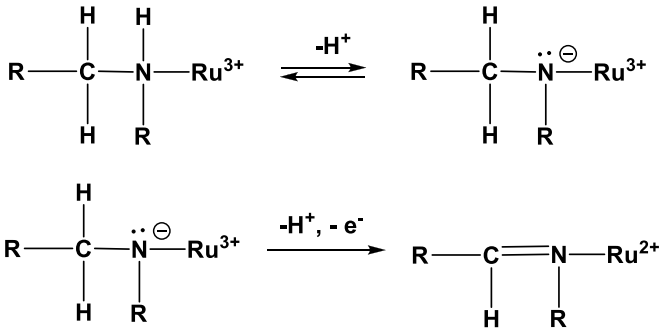

Scheme 3. Taube's accepted amine to imine formation starting from Ru^{3+} amine complexes. [66]

For our 15aneN5 system, this process would need to occur twice and may involve uncomplexed Ruthenium ions as a source/sink of electrons. Bound Ru^{2+} would be re-oxidized back to Ru^{3+} to allow imine formation via the same route for the second imine. The complexation reaction produces uncharacterized black solid assigned as Ru^{o}, which would indicate uncomplexed Ruthenium is involved. The yield is also less than 50%, and Ru^{o} precipitation would account for this limited amount of product.

3) **Ruthenium and Tetraaza Amine/Imine Macrocycles**

The ubiquitous tetraazamacrocycles cyclam (14aneN4)[67-70] and cyclen (12aneN4)[71, 72] have produced $Ru^{2+/3+}$ complexes with chloride monodentate ligands and are the closest analogues to [Ru(**15aneN5-diimine**)Cl](PF_6). Both the *cis*[54, 69] and *trans*[67, 68] isomers of [Ru(**cyclam**)Cl_2]$^+$ have been structurally characterized, with no imine formation present. However, Taube observed from a synthesis using $K_2[RuCl_5(H_2O)]$ as the metal source, that the primary but not structurally characterized product likely contained an oxidized imine ligand, with a C=N IR band at 1615 cm^{-1} present.[68] In this same paper, it was noted that larger macrocycles, **15aneN4** and **16aneN4**, appear to favour imine formation as well, which may be due to matching the larger Ru^{2+} vs smaller Ru^{3+} ionic radius. Obviously, **15aneN5** is in the same size range.

Cyclen complexes with Ru include *cis*-[Ru(**cyclen**)Cl_2]Cl,[71] which was not structurally characterized, *cis*-[Ru(**cyclen**)(L)]$^+$,[60, 73] where L = bipy, phen, and 4-NCpy, which were also not structurally characterized. In this paper, "oxidative dehydrogenation" to form at least one imine bond was noted at high pH—the ligand produced, though not structurally characterized, was named **imcyclen**. An IR band at 1630 cm^{-1} was cited as evidence of the imine group produced, and NMR spectra indicated only a single imine bond was formed. *cis*-[Ru(**imcyclen**)Cl(NO^+)]$^{2+}$, was reported,[72] but again not structurally characterized, from *cis*-[Ru(**cyclen**)Cl_2]Cl as starting material. An IR band at 1612 cm^{-1} was observed for the C=N group.

Finally, a structurally characterized *cis*-[Ru(**imcyclen**)] complex was published by Fujita in 2013 as a capping group for a "molecular capsule".[61] This remains the only structurally characterized imine containing cyclam or cyclen complex of Ruthenium, and was compared to the structural features of [Ru(**15aneN5-diimine**)Cl](PF_6) above. Below, we will compare other, non-structural properties of [Ru(**15aneN5-diimine**)Cl](PF_6) with those of the Ru cyclam-imine and cyclen-imine complexes previously published.

4) **Characterization of [Ru(15aneN5-diimine)Cl](PF_6)**.

Although the "parent" cyclam and cyclen complexes have been structurally characterized with ruthenium in a number of cases, there appears to be only one imine containing cyclen crystal structures for comparison to [Ru(**15aneN5-diimine**)Cl](PF_6) (see above). Perhaps it is the larger ring size, as noted by Taube[68] that favours the Ru^{2+} complex and allowed our **15aneN5-diimine** structural characterization. Addition characterization of this complex has been obtained and will be discussed here, and compared to primarily the cis-[Ru(**imcyclen**)Cl(NO^+)]$^{2+}$,[72] and to Fujita's structurally characterized Ru(**imcyclen**) complex.[61]

First an IR band at 1623 cm^{-1} was observed for [Ru(**15aneN5-diimine**)Cl](PF_6) and assigned to the C=N bonds, which match well with the similarly assigned IR bands of all of the imine groups listed above. The magnetic behaviour of [Ru(**15aneN5-diimine**)Cl](PF_6) was determined as diamagnetic, which allowed the collection of proton and carbon NMR spectra. ^{1}H NMR in CD_3CN gave a signal at δ = 8.64 ppm (s, 2H), assigned as the imine C-H protons, which is good agreement with [Ru(**imcyclen**)Cl(NO^+)]$^{2+}$, for which the imine proton is assigned δ = 8.1 ppm.[72] Similarly, Fujita assigns a δ = 8.38-8.64 ppm to his imine protons.[61] The [Ru(**15aneN5-diimine**)Cl](PF_6) ^{13}C NMR spectrum in CD_3CN gave a signal at δ = 155.58 ppm, which was assigned as the imine carbons. Fujita assigns δ = 171.1 and 171.3 ppm to his imine carbons.[61]

A UV-Visible spectrum in acetonitrile was obtained for [Ru(**15aneN5-diimine**)Cl](PF_6) and gave the following peaks: λ_{max} = 237 nm, ε = 6,460 $M^{-1}cm^{-1}$; λ_{max} = 437 nm; ε = 4,040 $M^{-1}cm^{-1}$; λ_{max} = 691 nm; ε = 97 $M^{-1}cm^{-1}$. The two higher energy absorptions are clearly charge transfer in nature as seen by the large extinction coefficients. The 691 nm absorbance appears to be a forbidden d-d band with an extinction coefficient below 100 $M^{-1}cm^{-1}$. These observations are consistent with a low spin distorted octahedral d^6 Ru^{2+} complex.[74] [Ru(**imcyclen**)Cl(NO^+)]$^{2+}$, gave bands at 350 nm and 450 nm and were assigned to overlapping charge transfer and d-d bands[72]—although the charge transfer bands were assigned to the NO ligand, which makes comparison here difficult. For the poorly characterized cyclam, 15aneN4, and 16aneN4 imine-containing Ru complexes of Taube, absorptions between 480-490 nm with high (but not calculated) extinctions coefficients were noted for the undesired imine products, but detailed spectra or values were not given.[68] Fujita does not give UV-Visible spectrum data, which would be very complex as the large capsule compounds contain multiple Ru centres and aromatic amine ligands.[61]

Finally, cyclic voltammetry in acetonitrile of [Ru(**15aneN5-diimine**)Cl](PF_6) was obtained and gave the following results: a reversible couple was seen at $E_{1/2}$ ($Ru^{2+/3+}$) = +0.640 V vs SHE with a peak separation of 95 mV. An additional irreversible reduction at E_{red} = -1.048 V vs SHE was observed and assigned to a reduction to Ru^+. These values make sense for a stabilized Ru^{2+} ion that requires a significant positive oxidation potential to oxidize to Ru^{3+}. The reversibility indicates that both oxidation states are stable with this ligand set, at least under the time scale of the experiment. Reduction to Ru^+ seems logical in a large, mostly neutral macrocycle pocket, but is likely made difficult (as shown by the large negative potential needed) by the presence of the Cl- ligand, which likely dissociates upon reduction and accounts for the irreversibility of the process. [Ru(**imcyclen**)Cl(NO^+)]$^{2+}$ cyclic voltammetry was obtained, but only exhibited electrochemical process associated with the NO ligand, while the Ru^{2+} ion was not oxidized or reduced. Fujita does not give cyclic voltammetry data.[61]

5) **Ru Case Study Conclusions**

Although only one tetraazamacrocycle imine complexes of Ruthenium has been structurally characterized,[61] the parent tetraazamacrocycles cyclam and cyclen complexes have been synthesized and show a distinct tendency towards ligand oxidation to imines. It is perhaps not surprising that the 15aneN5 macrocycles would react similarly. However, the complex [Ru(**15aneN5-diimine**)Cl](PF_6) was easily isolated and fully characterized, while the tetraazamacrocycle analogues were generally difficult to isolate and fully characterize. Perhaps the pentacoordinate ligand and large ring size are advantageous for being able to stabilize the large Ru^{2+} ion in an imine environment. We hope this case study comparison demonstrates the potential of the pentaazamacrocycles for extending the coordination chemistry of the tetraazamacrocycles.

Conclusions

This study has focused on the evolving synthesis of **15aneN5**, its transition metal complexes, and the X-ray crystal structure characterization of both intermediates in the ligand synthesis as well as the metal complexes produced. An alternate synthesis of **15aneN5** has been developed that uses less specialized synthetic equipment and processes (such as Schlenk filters and Soxhlet extractors), bypasses multiple-day drying and extracting processes shortening the full synthesis by many days. Combined, these changes slightly lower the yields, but make the synthesis shorter, simpler, and accessible to even undergraduate laboratory students. X-ray crystallography of multiple novel complexes included the first crystal structures of **15aneN5** with Cr^{3+}, Mn^{3+}, Fe^{3+}, Co^{3+}, Cu^{2+}, and Ru^{2+}, the latter ion bound to a novel diimine macrocycle that formed during the complexation of **15aneN5** with Ru^{3+}. This latter complex was fully characterized and compared to the scant data available for analagous tetraazamacroycle derived (cyclam and cyclen) Ruthenium-imine complexes to illustrate the potential for extending known tetraazamacrocycle coordination chemistry studies to the pentaazamacrocycles. Finally, a parameter to quantify the coordination geometry adopted by the ligand, designated the T-factor, was devised and applied to all known crystal structures of its metal complexes. We are optimistic that simplifying the **15aneN5** synthesis, broadening the list of transition metal ions complexed and structurally characterized to it, and quantifying the coordination geometries observed will lead to increased use and novel applications of pentaazamacrocycle ligand complexes.

Experimental Section

General:

N,N′-bis(2-hydroxyethyl)-ethylenediamine, Tosyl Chloride, and N,N′,N″-Tris(p-tolylsulfonyl)-diethylenetriamine disodium salt were purchased from Aldrich. Glyoxal (40% wt in water), methyl iodide (99%), and sodium borohydride (98%) were purchased from Aldrich Chemical Co. All solvents were of reagent grade and were dried, when necessary, by accepted procedures. Elemental analyses were performed by on a Perkin-Elmer EA2400 elemental analyzer. Electrospray Mass spectra were collected on a Shimadzu LCMS 2020 Electrospray Mass Spectrometer. NMR spectra were obtained on a Varian Bruker AVANCE II 300 MHz NMR Spectrometer instrument. IR spectra of the samples as KBr pellets were recorded on a Thermo-Nicolet 380 FTIR Spectrometer. Electronic spectra were recorded using a Shimadzu UV-240 UV-Vis Spectrometer. Magnetic moments were obtained on finely ground solid samples at ambient temperatures using a Johnson Matthey MSB Auto magnetic susceptibility balance. Electrochemical experiments were performed on a BAS100B Electrochemical Analyzer. A button Pt electrode was used as the working electrode with a Pt-wire counter electrode and a Ag-wire pseudo-reference electrode. Scans were taken at 200 mV/s. Acetonitrile solutions of the complexes (1 mM) with tetrabutylammonium hexafluorophosphate (0.1 M) as a supporting electrolyte were used. The measured potentials were referenced to SHE using ferrocene (+0.400 V versus SHE) as an internal standard. All electrochemical measurements were carried out under N_2.

Modified[48] synthesis of 1,4,7,10,13-pentaazacyclopentadane.

N,N′,O,O′-Tetrakis(p-tolylsulfonyl)-3,6-diazaoctane-1,8-diol (**2**). A cloudy solution of 76.26 g (0.400 mol) of p-toluenesulfonyl chloride in 180 ml of dichloromethane were added dropwise, over the course of one hour, to an ice-water bath cooled (~5 °C) suspension of 14.82 g (0.100 mol) of N,N′-bis(2-hydroxyethyl)-ethylenediamine (**1**), and 70 ml triethylamine in 80 ml of dichloromethane. After addition was complete, the ice water bath was allowed to come to room temperature as the reaction was stirred overnight (~16 hours). The cloudy slightly yellow suspension was washed once with 600 ml deionized water, twice with 200 ml of 1 M HCl, twice with 200 ml of saturated $NaHCO_3$, and twice with 200 mol of saturated NaCl. The dichloromethane layer was dried overnight with Na_2SO_4, which was then filtered off and the solvent evaporated. The yellow solid was dried under high vacuum for 30 minutes and then broken up in 400 ml anhydrous ethanol. The suspended solid was filtered open to the air on a medium fritted funnel, washed twice with 100 ml additional anhydrous ethanol, and dried under vacuum. Yield: 55.73 g (73%). $ESMS^+$ (50%MeOH/50%H_2O): m/z = 810 (Na_2L^+); m/z = 787 (NaL^+); m/z = 633 [Na(L-OTs)$^+$]; and m/z = 453 (L-2OTs$^+$). ^1H NMR ($CDCl_3$, 300 MHz) δ 7.74 (m, 8H), 7.35 (d, 8H), 4.14 (t, 4H), 3.37 (t, 4H), 3.30 (s, 4H), 2.44 (s, 12H). ^{13}C NMR ($CDCl_3$, 75 MHz) δ 145.20, 143.76, 134.98, 132.35, 130.07, 127.99, 127.35, 68.99, 49.86, 49.46, 21.68, 21.57. Anal. Calcd for $C_{34}H_{40}N_2O_{10}S_4$: C 53.38; H 5.27; N 3.66; Found: C 53.29; H 5.12; N 4.01. X-ray quality crystals were obtained from a 1:1 MeOH:H_2O solution. See ESI for discussion of the crystal structure.

1,4,7,10,13-Pentakis(p-toluensulfonyl)-1,4,7,10,13-pentaazapentadecane (4). 54.00 g (0.0707 mol) of (**2**) was dissolved in 430 ml of DMF and added to an addition funnel. One equivalent (43.04 g, 0.0707 mol) of N, N′, N′′-Tris(p-tolylsulfonyl)-diethylenetramine disodium salt (**3**) was dissolved in 1290 ml of DMF in a 2 L roundbottom flask, and under nitrogen, heated to 105 °C. The solution of (**2**) was added over a period of 5 hours and the reaction solution allowed to continue stirring at 105 °C for an additional 12 hours. The cooled solution was evaporated on a rotary evaporator until solid began to precipitate at about 1/3 its initial volume. This solution was then added to 1500 ml ice cold deionized water with stirring to produce copious white precipitate. The solid was filtered on a medium glass frit and washed three times with 500 ml portions of ice cold deionized water. The solid product was then dissolved through the frit into a clean filter flask with 5 x 200 ml portions of boiling acetonitrile to give a dark yellow solution. Polymers remained on the frit. The acetonitrile solution was rotary evaporated to 200 ml and set in a freezer overnight to precipitate the product. The product was obtained by filtration on a glass frit open to the air. A second fraction was obtained by rotary evaporating the filtrate to 100 ml and storing in the freezer overnight again. Both fractions were combined and dried overnight under vacuum. Yield: 29.98 g (43%). $ESMS^+$ (50%MeOH/50%H_2O): m/z = 832 (L-OTs)$^+$. ^1H NMR ($CDCl_3$, 300 MHz) δ 7.67 (d, 10H), 7.33 (d, 10H), 3.27 (s, 20H), 2.44 (s, 15H). ^{13}C NMR ($CDCl_3$, 75 MHz) δ 144.05, 134.86, 129.99, 127.44, 49.63, 21.59. Anal. Calcd for $C_{45}H_{55}N_5O_{10}S_5$: C 54.80; H 5.62; N 7.10; Found: C 54.92; H 5.50; N 6.95.

N, N′, N′′-Tris(p-tolylsulfonyl)-diethylenetramine (**3′**). N, N′, N′′-Tris(p-tolylsulfonyl)-diethylenetramine disodium salt (**3**) was purchased from Sigma-Aldrich and used without purification. On several occasions, after the reaction above to produce (**4**) some residual DMF solution containing (**3**) produced X-ray quality crystals of (**3′**), the neutral organic compound. See ESI for discussion of the crystal structure.

1,4,7,10,13-pentaazapentadecane (15aneN5). 30.00 g (0.0304 mol) of (**4**) was suspended in 240 ml conc. H_2SO_4 in a 2 L three-neck roundbottom flask. The mixture was heated to 180 °C and held at this temperature for 25 minutes, during which time all solid reactant dissolved to form a dark brown or black solution. The solution was cooled in an ice bath and 1050 ml diethyl ether were added over 30 minutes with stirring to precipitate a gray/black semisolid polyhydrosulfate salt. The semisolid was filtered on a medium glass

frit open to the air and washed three times with 100 ml diethyl ether. The semisolid was dissolved through the frit in to a clean filter flask with deionized water (300 ml total in several portions). 200 ml 6 M NaOH was added to bring the pH to 13. Five extractions with 100 ml $CHCl_3$ were followed by drying the organic layer with Na_2SO_4, filtration, and solvent removal to yield the pure, white product. Yield: 4.01 g (61%). $ESMS^+$ (50%MeOH/50%H_2O): m/z = 216 (LH^+). ^1H NMR ($CDCl_3$, 300 MHz) δ 2.65 (s, 20H), 2.09 (br s, 5H). ^{13}C NMR ($CDCl_3$, 75 MHz) δ 48.59. Anal. Calcd for $C_{10}H_{25}N_5$. 0.1 H_2O: C 55.46; H 11.69; N 32.12; Found: C 55.53; H 11.93; N 31.73. X-ray quality crystals of the neutral compound appeared to form at the top of a roundbottom flask of product that dried overnight under high vacuum. X-ray quality crystals of [H_3(**15aneN5**)]$Cl_2(PF_6)$ were obtained as a byproduct of a Cr complexation reaction and were obtained from pentane diffusion into a methanol solution. See ESI for discussion of the crystal structures.

General Procedure for Metal Complexation.

In an inert atmosphere glovebox, 0.323 g (0.0015 mol) of **15aneN5** and one equivalent (0.0015 mol) of the respective anhydrous metal salt were stirred overnight at room temperature in 10 ml anhydrous MeOH in a 4-dram vial. Individual metal complex details for workup and characterization given below.

[Cr(15aneN5)Cl]Cl(PF_6): $CrCl_3$, 0.238 g. The reaction solution was removed from the glovebox and filtered to remove minimal solids. 5 eq. of NH_4PF_6 (1.223 g, 0.0075 mol) were added with stirring to the filtrate to produce a pink powder precipitate. The suspension was stored for 30 minutes at -10 °C to complete precipitation. The pink powder product was obtained by filtration on a fine glass frit, washed with minimal cold MeOH and then diethyl ether and vacuum dried. Yield: 0.515 g (71%). $ESMS^+$ (50%MeOH/50%H_2O): m/z = 301 ($CrLCl^+$); m/z = 337 ($CrLCl_2^+$). Anal. Calcd for $Cr(C_{10}H_{25}N_5)Cl_{2.1}(PF_6)_{0.9}$: C 25.43; H 5.34; N 14.83; Found C 25.60; H 5.41; N 14.99. X-ray quality crystals were grown from ether diffusion into a methanol solution. A second X-ray quality red-purple plate were obtained from pentane diffusion into nitromethane and had only chloride counterions and no PF_6^- in the structure.

[Mn(15aneN5)(H_2O)](PF_6)$_2$: $Mn(OAc)_2$, 0.260 g. The reaction solution was removed from the glovebox and filtered to remove minimal solids. 5 eq. of NH_4PF_6 (1.223 g, 0.0075 mol) were added with stirring to the filtrate to produce a tan powder precipitate. The suspension was stored for 30 minutes at -10 °C to complete precipitation. The tan powder product was obtained by filtration on a fine glass frit, washed with minimal cold MeOH and then diethyl ether and vacuum dried. Yield: 0.199 g (23%). $ESMS^+$ (50%MeOH/50%H_2O): m/z = 270 (MnL^+); m/z = 287 ($MnL(OH_2)^+$). Anal. Calcd for $Mn(C_{10}H_{25}N_5)(H_2O)(PF_6)_2$: C 20.77; H 4.71; N 12.11; Found C 21.25; H 4.74; N 11.93. X-ray quality crystals were grown from cooling a propanol solution, and clearly show an NH_3 ligand in place of the water formulated above. This ammonia could come from the NH_4PF_6 salt used to precipitate the complex, and appears not to be present in the bulk complex, according to the elemental analysis. It is possible that the ammonia complex may be a small part of the sample, or forms only under the specific conditions under which the crystal grew.

[Fe(15aneN5)Cl_2]: $FeCl_2$, 0.260 g. This reaction was carried out in DMF. The reaction solution was removed from the glovebox and filtered to remove minimal solids. The filtrate was evaporated under vacuum to give a brown solid which was vacuum dried. Yield: 0.451 g (77%). $ESMS^+$ (50%MeOH/50%H_2O): m/z = 341 ($FeLCl_2^+$); m/z = 305 ($FeLCl^+$). Anal. Calcd for $Fe(C_{10}H_{25}N_5)Cl_2$. 1.3DMF: C 38.19; H 7.86; N 20.19; Found C 38.10; H 8.23; N 21.45. X-ray quality crystals were grown from diffusion of ether into a DMF solution.

[Fe(15aneN5)(OAc)$_2$](PF_6): $Fe(OAc)_2$, 0.261 g. The reaction solution was filtered to remove minimal solids. 5 eq. of NH_4PF_6 (1.223 g, 0.0075 mol) were added with stirring to the filtrate in the glovebox, and then the pale yellow solution removed from the glovebox, but protected from air. In a hood (CAUTION: Br_2 is toxic!) the reaction solution was opened under a stream of nitrogen and 10 drops of Br_2 was added by pipet. Yellow precipitate formed immediately. Nitrogen was bubbled through the solution in the hood for 10 minutes to remove excess bromine. The suspension was stored for 30 minutes at -10 °C to complete precipitation. The yellow powder product was obtained by filtration on a fine glass frit, washed with minimal cold MeOH and then diethyl ether and vacuum dried. Yield: 0.440 g (62%). $ESMS^+$ (50%MeOH/50%H_2O): m/z = 391 ($FeL(OAc)_2^+$); m/z = 330 ($FeL(OAc)^+$). Anal. Calcd for $Fe(C_{10}H_{24}N_5)(C_2H_3O_2)_{1.5}(PF_6)_{1.5}$: C 27.10; H 4.99; N 12.15; Found C 27.48; H 5.25; N 12.40. X-ray quality crystals were grown from pentane diffusion into a 2-butanane solution.

[Co(15aneN5)Cl]Cl: $CoCl_2$, 0.195 g. This reaction was carried out in DMF. The reaction solution was removed from the glovebox and filtered to remove minimal solids. The filtrate was evaporated under vacuum to give a blue solid which was vacuum dried. Yield: 0.304 g (59%). $ESMS^+$ (50%MeOH/50%H_2O): m/z = 272 (CoL^+); m/z = 309 ($CoLCl^+$). Anal. Calcd for $Co(C_{10}H_{25}N_5)Cl_2$. 1.65H_2O: C 32.04; H 7.61; N 18.68; Found C 32.44; H 7.42; N 18.23. Three different Co^{2+} crystal structures were obtained. X-ray quality aquamarine blocks were grown from diffusion of ether into a MeOH solution. Additional, different X-ray quality aquamarine blocks were grown from ether diffusion in to DMF. Additional, different X-ray quality peach blocks were grown from ether diffusion into DMF.

[Ni(15aneN5)(OAc)](PF_6): $Ni(OAc)_2$, 0.265 g. The violet reaction solution was removed from the glovebox and filtered to remove minimal solids. 5 eq. of NH_4PF_6 (1.223 g, 0.0075 mol) were added with stirring to the filtrate to produce a violet powder precipitate. The suspension was stored for 30 minutes at -10 °C to complete precipitation. The violet powder product was obtained by filtration on a fine glass frit, washed with minimal cold MeOH and then diethyl ether and vacuum dried. Yield: 0.483 g (67%). $ESMS^+$ (50%MeOH/50%H_2O): m/z = 272 (NiL^+); m/z = 332 ($NiL(OAc)^+$). Anal. Calcd for $Ni(C_{10}H_{25}N_5)(C_2H_3O_2)(PF_6)$: C 30.15; H 5.90; N 14.65; Found C 30.05; H 5.73; N 14.56. X-ray quality crystals were grown from ether diffusion into an acetonitrile solution.

[Cu(15aneN5)](PF_6)$_2$: $Cu(OAc)_2$, 0.272 g. The deep blue-purple reaction solution was removed from the glovebox and filtered to remove minimal solids. 5 eq. of NH_4PF_6 (1.223 g, 0.0075 mol) were added with stirring to the filtrate to produce a deep blue-purple precipitate. The suspension was stored for 30 minutes at -10 °C to complete precipitation. The deep blue-purple powder product was obtained by filtration on a fine glass frit, washed with minimal cold MeOH and then diethyl ether and vacuum dried. Yield: 0.632 g (74%). $ESMS^+$ (50%MeOH/50%H_2O): m/z = 277 (CuL^+); m/z = 139 (CuL^{+2}); m/z = 155 ($CuL(MeOH)^{2+}$. Anal. Calcd for $Cu(C_{10}H_{25}N_5)(PF_6)_2$: C 21.12; H 4.43; N 12.31; Found C 21.00; H 4.21; N 12.09. X-ray quality crystals were grown from ether diffusion into a nitromethane solution.

[Zn(15aneN5)](PF_6)$_2$: $Zn(OAc)_2$, 0.275 g. The colorless reaction solution was removed from the glovebox and filtered to remove minimal solids. 5 eq. of NH_4PF_6 (1.223 g, 0.0075 mol) were added with stirring to the filtrate to produce a white precipitate. The suspension was stored for 30 minutes at -10 °C to complete precipitation. The white powder product was obtained by filtration on a fine glass frit, washed with minimal cold MeOH and then diethyl ether and vacuum dried. Yield: 0.545 g (64%). $ESMS^+$ (50%MeOH/50%H_2O): m/z = 278 (ZnL^+); m/z = 296 ($ZnL(H_2O)^+$); m/z

= 140 (ZnL^{+2}); m/z = 156 ($ZnL(MeOH)^{2+}$). Anal. Calcd for $Zn(C_{10}H_{25}N_5)(PF_6)_2$: C 21.05; H 4.42; N 12.27; Found C 20.98; H 4.28; N 12.11. X-ray quality crystals were grown from ether diffusion into a 2-butanone solution. ^{1}H NMR (CD_3CN, 300 MHz) δ 3.48 (br s, 1H), 3.07 (m, 9H), 2.93 (m, 4H), 2.67 (m, 6H), 2.46 (m, 3H), 2.34 (m, 2H). ^{13}C NMR (CD_3CN, 75 MHz) δ 46.88 (s, 2C), 45.78 (br s, 6C), 45.30 (s, 2C).

[Ru(15aneN5-diimine)Cl](PF$_6$): $RuCl_3$. $1.6H_2O$, 0.354 g. The dark green reaction solution was removed from the glovebox and filtered to remove trace solids. 5 eq. of NH_4PF_6 (1.223 g, 0.0075 mol) were added with stirring to the filtrate to produce a dark green precipitate. The suspension was stored for 30 minutes at -10 °C to complete precipitation. The dark green powder product was obtained by filtration on a fine glass frit, washed with minimal cold MeOH and then diethyl ether and vacuum dried. Yield: 0.337 g (46%). $ESMS^+$ (50%MeOH/50%H_2O): m/z = 438 ($RuLCl^+$). Anal. Calcd for $[Ru(C_{10}H_{21}N_5)Cl](PF_6)$. $1H_2O$: C 23.51; H 4.54; N 13.71; Found C 23.20; H 4.36; N 13.53. X-ray quality crystals were grown from pentane diffusion into an acetone solution. ^{1}H NMR (CD_3CN, 300 MHz) δ 8.64 (s, 2H), 5.55 (br s, 3H), 4.16 (dd, 2H), 3.65 (m, 2H), 3.61 (m, 2H), 3.46 (m, 4H), 2.81 (m, 2H), 2.65 (m, 2H), 2.48 (m, 2H). ^{13}C NMR (CD_3CN), 75 MHz) δ 155.58, 56.96, 54.69, 53.48, 49.68, 46.12.

Crystallographic details

CCDC 2101507-2101522 contain the supplementary crystallographic data for this paper. These data can be obtained free of charge from The Cambridge Crystallographic Data Centre via www.ccdc.cam.ac.uk/structures

Single-crystal X-ray diffraction data were collected using synchrotron radiation. Crystallographic data were collected through the SCrALS (Service Crystallography at Advanced Light Source) program at the Small-Crystal Crystallography Beamline 11.3.1 at the Advanced Light Source (ALS), Lawrence Berkeley National Laboratory. The ALS is supported by the U.S. Department of Energy, Office of Energy Sciences Materials Sciences Division, under contract DE-AC02-05CH11231.

Intensity data were collected at 150K on a D8 goniostat equipped with a Bruker PHOTON100 CMOS detector at Beamline 11.3.1 at the Advanced Light Source (Lawrence Berkeley National Laboratory) using synchrotron radiation tuned to λ = 0.7749 Å. In a typical data, collection frames were measured for a duration of 1s at 0.5° intervals of ω. The data frames were collected using the program APEX2 and processed using the program SAINT routine within APEX2.[75] The data were corrected for absorption and beam corrections based on the multi-scan technique as implemented in SADABS.[76]

Structures were solved and refined within Olex2 using SHELXT[77] and SHELXL-2018. It was common to observe disorder in the position so hexafluorophosphate anions. This was modelled using standard procedures including restraints on chemically identical parts. Hydrogen atoms were placed using a riding model and where electron density maps indicated it was reasonable, X-H bond lengths were refined. Crystal data and structure refinement details are given in Tables 2-5 below.

Identification code	dd07a cmca	ALB04
Empirical formula	$C_{13.76}H_{30.64}F_6FeI_{0.12}N_5O_{3.76}P$	$C_{10}H_{25}Cl_2FeN_5$
Structural formula	[Fe(**15aneN5**)$(CH_3COO)_2$](PF_6)	[Fe(**15aneN5**)Cl_2]
Formula weight	542.40	342.10
Temperature/K	150	150
Crystal system	orthorhombic	monoclinic
Space group	*Cmce*	$P2_1/n$
a/Å	17.9648(14)	7.9184(6)
b/Å	19.2765(14)	6.7907(5)
c/Å	12.8235(10)	14.7266(11)
α/°	90	90
β/°	90	100.133(2)
γ/°	90	90
Volume/Å^3	4440.8(6)	779.52(10)
Z	8	2
ρ_{calc}g/cm^3	1.623	1.457
μ/mm^{-1}	1.253	1.642
F(000)	2237.0	360.0
Crystal size/mm^3	0.07 × 0.05 × 0.03	0.04 × 0.02 × 0.02
Radiation / Å	synchrotron (λ = 0.7749)	synchrotron (λ = 0.7749)
2Θ range for data collection/°	4.608 to 62.35	5.976 to 62.27
Index ranges	-24 ≤ h ≤ 23, -25 ≤ k ≤ 25, -17 ≤ l ≤ 17	-10 ≤ h ≤ 10, -9 ≤ k ≤ 9, -19 ≤ l ≤ 19
Reflections collected	28456	15568
Independent reflections	2871 [R_{int} = 0.0429, R_{sigma} = 0.0233]	1936 [R_{int} = 0.0378, R_{sigma} = 0.0201]
Data/restraints/parameters	2871/219/204	1936/274/157
Goodness-of-fit on F^2	1.033	1.061
Final R indexes [I>=2σ (I)]	R_1 = 0.0528, wR_2 = 0.1538	R_1 = 0.0203, wR_2 = 0.0515
Final R indexes [all data]	R_1 = 0.0640, wR_2 = 0.1651	R_1 = 0.0231, wR_2 = 0.0529
Largest diff. peak/hole / e Å^{-3}	0.92/-0.55	0.45/-0.30

Table 2: Crystal data and structure refinement details for 7-coordinate complexes

Identification code	KS11	JE07	MG07B P1
Empirical formula	$C_{12}H_{31}CuF_{12}N_7O_4P_2$	$C_{10}H_{25}F_{12}N_5P_2Zn$	$C_{10}H_{21}ClF_6N_5PRu$
Structural formula	[Cu(**15aneN5**)]$(PF_6)_2(CH_3NO_2)_2$	[Zn(**15aneN5**)]Cl_2	[Ru(**15aneN5-diimine**)Cl](PF_6)
Formula weight	690.92	570.66	492.81
Temperature/K	150	150	150
Crystal system	monoclinic	monoclinic	triclinic
Space group	$P2_1$	$I2/a$	P-1
a/Å	8.2222(4)	12.6817(10)	7.7456(7)
b/Å	12.5513(7)	25.670(3)	10.3834(9)
c/Å	12.9958(7)	12.8729(10)	11.0010(10)
α/°	90	90	75.896(2)
β/°	104.977(2)	106.102(7)	88.525(2)
γ/°	90	90	85.227(2)
Volume/Å^3	1295.60(12)	4026.2(7)	855.10(13)
Z	2	8	2
ρ_{calc}g/cm^3	1.771	1.883	1.914
μ/mm^{-1}	1.372	1.887	1.538
F(000)	702.0	2304.0	492.0
Crystal size/mm^3	0.06 × 0.04 × 0.025	0.04 × 0.03 × 0.03	0.04 × 0.03 × 0.015
Radiation / Å	synchrotron (λ = 0.7749)	synchrotron (λ = 0.7749)	synchrotron (λ = 0.7749)
2Θ range for data collection/°	3.538 to 62.186	4.35 to 62.334	4.162 to 62.298
Index ranges	-10 ≤ h ≤ 10, -16 ≤ k ≤ 16, -17 ≤ l ≤ 17	-16 ≤ h ≤ 16, -34 ≤ k ≤ 34, -17 ≤ l ≤ 17	-10 ≤ h ≤ 10, -13 ≤ k ≤ 13, -14 ≤ l ≤ 14
Reflections collected	47487	26484	11091
Independent reflections	6354 [R_{int} = 0.0511, R_{sigma} = 0.0572]	5002 [R_{int} = 0.0634, R_{sigma} = 0.0528]	4249 [R_{int} = 0.0310, R_{sigma} = 0.0348]
Data/restraints/parameters	6354/754/458	5002/246/319	4249/331/257
Goodness-of-fit on F^2	1.120	1.067	1.029
Final R indexes [I>=2σ (I)]	R_1 = 0.0355, wR_2 = 0.0699	R_1 = 0.0628, wR_2 = 0.1758	R_1 = 0.0235, wR_2 = 0.0604
Final R indexes [all data]	R_1 = 0.0360, wR_2 = 0.0702	R_1 = 0.0788, wR_2 = 0.1896	R_1 = 0.0258, wR_2 = 0.0618
Largest diff. peak/hole / e Å^{-3}	0.65/-0.60	1.34/-0.63	0.50/-0.45
Flack parameter	0.44(9)	none	none

Table 3: Crystal data and structure refinement details for 5-coordinate complexes of **15aneN5** and [Ru(**15aneN5**-diimine)Cl](PF_6)

Identification code	DGJ07B P-1	DR08 Cc	MBA09	DSB04A P212121	DSB04B_C2onC	DSB04C-Pbca	AF07 P212121
Empirical formula	$C_{10}H_{25}Cl_2CrF_6N_5P$	$C_{10}H_{27}Cl_3CrN_5O$	$C_{10}H_{28}F_{12}MnN_6P_2$	$C_{10}H_{25}Cl_4Co_2N_5$	$C_{20}H_{50}Cl_6Co_3N_{10}$	$C_{10}H_{25}Cl_2CoN_5$	$C_{12}H_{28}F_6N_5NiO_2P$
Structural formula	[Cr(**15aneN5**)Cl]Cl(PF_6)	[Cr(**15aneN5**)Cl]Cl_2(H_2O)	[Mn(**15aneN5**)NH_3](PF_6)	[Co(**15aneN5**)]-μCl-[$CoCl_3$]	[Co(**15aneN5**)Cl]$_2$[$CoCl_4$]	[Co(**15aneN5**)Cl]Cl	[Ni(**15aneN5**)(CH_3COO)](PF_6)
Formula weight	483.22	391.71	577.26	475.01	820.19	345.18	478.07
Temperature/K	150	150	150	150	150	150	150
Crystal system	triclinic	monoclinic	hexagonal	orthorhombic	monoclinic	orthorhombic	orthorhombic
Space group	*P*-1	*Cc*	$P6_5$	$P2_12_12_1$	*C*2/*c*	*Pbca*	$P2_12_12_1$
a/Å	9.0957(8)	15.3816(11)	9.1983(7)	8.6520(8)	14.6083(11)	14.5128(14)	9.8206(8)
b/Å	9.2333(9)	9.2277(11)	9.1983(7)	11.9224(10)	14.3727(11)	12.7676(11)	13.9643(11)
c/Å	22.464(2)	12.6805(11)	43.795(4)	18.0909(15)	16.8252(12)	32.102(3)	13.9819(11)
α/°	97.589(3)	90	90	90	90	90	90
β/°	93.469(2)	113.079(3)	90	90	103.155(3)	90	90
γ/°	96.344(2)	90	120	90	90	90	90
Volume/Å^3	1853.2(3)	1655.8(3)	3209.0(6)	1866.1(3)	3439.9(4)	5948.2(10)	1917.4(3)
Z	4	4	6	4	4	16	4
ρ_{calc}g/cm^3	1.732	1.571	1.792	1.691	1.584	1.542	1.656
μ/mm^{-1}	1.334	1.491	1.109	2.966	2.429	1.898	1.474
F(000)	988.0	820.0	1758.0	968.0	1692.0	2896.0	992.0
Crystal size/mm^3	0.04 × 0.025 × 0.015	0.05 × 0.03 × 0.015	0.07 × 0.04 × 0.03	0.06 × 0.02 × 0.02	0.04 × 0.025 × 0.02	0.05 × 0.04 × 0.03	0.05 × 0.04 × 0.02
Radiation / Å	synchrotron (λ = 0.7749)	synchrotron (λ = 0.7749)	synchrotron (λ = 0.7749)	synchrotron (λ = 0.7749)	synchrotron (λ = 0.7749)	synchrotron (λ = 0.7749)	synchrotron (λ = 0.7749)
2Θ range for data collection/°	4.888 to 62.188	5.746 to 62.274	5.576 to 62.378	4.462 to 62.242	4.392 to 62.318	4.126 to 55.292	4.494 to 62.36
Index ranges	-12 ≤ h ≤ 12, -12 ≤ k ≤ 12, -29 ≤ l ≤ 29	-20 ≤ h ≤ 20, -12 ≤ k ≤ 12, -16 ≤ l ≤ 16	-12 ≤ h ≤ 12, -12 ≤ k ≤ 12, -58 ≤ l ≤ 58	-11 ≤ h ≤ 11, -15 ≤ k ≤ 15, -23 ≤ l ≤ 24	-19 ≤ h ≤ 19, -19 ≤ k ≤ 19, -22 ≤ l ≤ 22	-17 ≤ h ≤ 17, -15 ≤ k ≤ 15, -38 ≤ l ≤ 38	-13 ≤ h ≤ 13, -18 ≤ k ≤ 18, -18 ≤ l ≤ 18
Reflections collected	36477	14520	38351	39234	34763	98328	25247
Independent reflections	9167 [R_{int} = 0.0462, R_{sigma} = 0.0437]	3952 [R_{int} = 0.0446, R_{sigma} = 0.0494]	5358 [R_{int} = 0.0626, R_{sigma} = 0.0430]	4616 [R_{int} = 0.0520, R_{sigma} = 0.0292]	4292 [R_{int} = 0.0584, R_{sigma} = 0.0319]	5348 [R_{int} = 0.1321, R_{sigma} = 0.0489]	4789 [R_{int} = 0.0483, R_{sigma} = 0.0324]
Data/restraints/parameters	9167/205/497	3952/15/194	5358/1299/384	4616/10/196	4292/10/182	5348/73/355	4789/10/251
Goodness-of-fit on F^2	1.050	1.044	1.024	1.043	1.034	1.034	1.059
Final R indexes [I>=2σ (I)]	R_1 = 0.0453, wR_2 = 0.1058	R_1 = 0.0296, wR_2 = 0.0552	R_1 = 0.0478, wR_2 = 0.1168	R_1 = 0.0238, wR_2 = 0.0602	R_1 = 0.0281, wR_2 = 0.0664	R_1 = 0.0416, wR_2 = 0.0836	R_1 = 0.0257, wR_2 = 0.0673
Final R indexes [all data]	R_1 = 0.0611, wR_2 = 0.1122	R_1 = 0.0355, wR_2 = 0.0570	R_1 = 0.0601, wR_2 = 0.1251	R_1 = 0.0259, wR_2 = 0.0612	R_1 = 0.0357, wR_2 = 0.0696	R_1 = 0.0742, wR_2 = 0.0958	R_1 = 0.0275, wR_2 = 0.0686
Largest diff. peak/hole / e Å^{-3}	0.79/-0.47	0.31/-0.31	0.53/-0.34	1.13/-0.26	0.55/-0.30	0.73/-0.49	0.42/-0.34
Flack parameter	none	0.014(11)	0.04(3)	0.014(12)	None	none	0.365(11)

Table 4: Crystal data and structure refinement details for 6-coordinate complexes of **15aneN5**

Identification code	GBMA01, intermediate **2**	EMAA02C, intermediate **3**	P-1 ADS102	DGJ07B2
Empirical formula	$C_{34}H_{40}N_2O_{10}S_4$	$C_{25}H_{31}N_3O_6S_3$	$C_{10}H_{25}N_5$	$C_{10}H_{28}Cl_2F_6N_5P$
Structural formula	$C_{34}H_{40}N_2O_{10}S_4$	$C_{25}H_{31}N_3O_6S_3$	**15aneN5**	(**15aneN5**H_3)Cl_2(PF_6)
Formula weight	764.92	565.71	215.35	434.24
Temperature/K	150	150	150	150
Crystal system	monoclinic	monoclinic	triclinic	monoclinic
Space group	$P2_1/n$	$P2_1/n$	P-1	$C2/c$
a/Å	5.7301(5)	5.1713(4)	4.9136(4)	18.619(2)
b/Å	18.6290(15)	27.181(2)	14.4136(11)	9.6164(8)
c/Å	16.8629(16)	18.8959(14)	17.9643(14)	11.7011(10)
α/°	90	90	92.224(2)	90
β/°	91.518(2)	93.137(2)	93.232(2)	110.806(4)
γ/°	90	90	92.069(2)	90
Volume/Å^3	1799.4(3)	2652.0(4)	1268.36(17)	1958.5(3)
Z	2	4	4	4
ρ_{calc}g/cm^3	1.412	1.417	1.128	1.473
μ/mm^{-1}	0.404	0.407	0.086	0.592
F(000)	804.0	1192.0	480.0	904.0
Crystal size/mm^3	0.07 × 0.03 × 0.03	0.05 × 0.05 × 0.04	0.1 × 0.03 × 0.01	0.08 × 0.07 × 0.01
Radiation / Å	synchrotron (λ = 0.7749)	synchrotron (λ = 0.7749)	synchrotron (λ = 0.7749)	synchrotron (λ = 0.7749)
2Θ range for data collection/°	4.768 to 55.286	4.028 to 62.326	4.956 to 62.206	5.104 to 57.88
Index ranges	-6 ≤ h ≤ 6, -22 ≤ k ≤ 22, -20 ≤ l ≤ 20	-6 ≤ h ≤ 6, -36 ≤ k ≤ 36, -25 ≤ l ≤ 25	-6 ≤ h ≤ 6, -19 ≤ k ≤ 19, -23 ≤ l ≤ 23	-23 ≤ h ≤ 21, -11 ≤ k ≤ 12, 0 ≤ l ≤ 14
Reflections collected	28467	48221	26198	3870
Independent reflections	3232 [R_{int} = 0.1156, R_{sigma} = 0.0497]	6577 [R_{int} = 0.0407, R_{sigma} = 0.0278]	6296 [R_{int} = 0.0409, R_{sigma} = 0.0364]	2002 [R_{int} = 0.0097, R_{sigma} = 0.0137]
Data/restraints/parameters	3232/0/307	6577/0/345	6296/50/299	2002/0/127
Goodness-of-fit on F^2	1.023	1.040	1.124	1.079
Final R indexes [I>=2σ (I)]	R_1 = 0.0351, wR_2 = 0.0850	R_1 = 0.0394, wR_2 = 0.0941	R_1 = 0.0534, wR_2 = 0.1319	R_1 = 0.0245, wR_2 = 0.0652
Final R indexes [all data]	R_1 = 0.0539, wR_2 = 0.0925	R_1 = 0.0535, wR_2 = 0.1010	R_1 = 0.0645, wR_2 = 0.1370	R_1 = 0.0264, wR_2 = 0.0664
Largest diff. peak/hole / e Å^{-3}	0.28/-0.32	0.40/-0.44	0.51/-0.28	0.29/-0.23

Table 5: Crystal data and structure refinement details for 2, 3, **15aneN5**, and (**15aneN5**H_3)Cl_2(PF_6)

Author Contributions

Anthony D. Shircliff, Investigation
Elisabeth M. A. Allbritton, Investigation
Dustin J. Davilla, Investigation
Michael-Joseph Gorbet, Investigation
Donald G. Jones, Investigation
David S. Tresp, Investigation
Michael B. Allen, Investigation
Alina Shrestha, Investigation
Gwendolyn E. Burgess, Investigation
John I. Eze, Investigation
Andrea T. Fernandez, Investigation
Daniel Ramirez, Investigation
Kody J. Shoff, Investigation
Garet G. Crispin, Investigation
Sarah B. Crone, Investigation
Michael Flinn, Investigation
Tien Tran, Investigation
Darby S. Bryce, Investigation
Abbagale L. Bond, Investigation
Dylan W. Shockey, Investigation
Allen G. Oliver, Data curation, Writing – review & editing, Resources, Investigation, Funding acquisition, Formal analysis
Jeanette A. Krause, Data curation, Writing – review & editing, Resources, Investigation, Funding acquisition, Formal analysis
Timothy J. Prior,* Data curation, Writing – original draft, Writing – review & editing, Visualization, Resources, Methodology, Investigation, Formal analysis, Conceptualization
Timothy J. Hubin,* Conceptualization, Data curation, Writing – original draft, Writing – review & editing, Visualization, Supervision, Resources, Project administration, Methodology, Investigation, Funding acquisition, Formal analysis

Conflicts of interest

There are no conflicts to declare.

Acknowledgements

Acknowledgment is made to the Donors of the American Chemical Society Petroleum Research Fund for support of this research. TJH thanks the Henry Dreyfus Teacher-Scholar Awards Program for support of this work. The Southwestern Oklahoma State University Department of Chemistry and Physics is acknowledged for support of CHEM 3211, Inorganic Chemistry Lab, where much of this work was carried out by undergraduates. Crystallographic data were collected through the SCrALS (Service Crystallography at Advanced Light Source) program at the Small-Crystal Crystallography Beamline 11.3.1 at the Advanced Light Source (ALS), Lawrence Berkeley National Laboratory. The ALS is supported by the U.S. Department of Energy, Office of Energy Sciences Materials Sciences Division, under contract DE-AC02-05CH11231.

Notes and references

1. B. Bosnich, C. K. Poon and M. L. Tobe, *Inorg. Chem.*, 1965, **4**, 1102-1108.
2. E. K. Barefield, *Coordination Chemistry Reviews*, 2010, **254**, 1607-1627.
3. G. McRobbie, G. C. Valks, C. J. Empson, A. Khan, J. D. Silversides, C. Pannecouque, E. De Clercq, S. G. Fiddy, A. J. Bridgeman, N. A. Young and S. J. Archibald, *Dalton Trans.*, 2007, 5008-5018.
4. T. E. Chanston and R. D. Hancock, *Inorganica Chimica Acta*, 1995, **230**, 165-167.
5. L. Y. Martin, L. J. DeHayes, L. J. Zompa and D. H. Busch, *Journal of the American Chemical Society*, 1974, **96**, 4046-4048.
6. P. V. Bernhardt, T. E. Dyahningtyas, S. C. Han, J. M. Harrowfield, I. C. Kim, Y. Kim, G. A. Koutsantonis, E. Rukmini and P. Thuery, *Polyhedron*, 2004, **23**, 869-877.
7. R. J. P. Corriu, F. Embert, Y. Guari, Y. Reye and R. Guilard, *Chem. Eur. J.*, 2002, **8**, 5732-5741.
8. G. R. Weisman, M. E. Rogers, E. H. Wong, J. P. Jasinski and E. S. Paight, *Journal of the American Chemical Society*, 1990, **112**, 8604-8605.
9. G. R. Weisman, E. H. Wong, D. C. Hill, M. E. Rogers, D. P. Reed and J. C. Calabrese, *Chem. Commun.*, 1996, 947-948.
10. T. J. Hubin, J. M. McCormick, S. R. Collinson, N. W. Alcock and D. H. Busch, *Chemical Communications*, 1998, 1675-1676.
11. T. J. Hubin, *Coord. Chem. Rev.*, 2003, **241**, 27-46.
12. C. M. May, S. J. Archibald, A. J. Bridgeman, C. J. Empson and T. J. Hubin, *Chemical Communications*, 2004, DOI: 10.1039/b405358c, 1880-1881.
13. T. J. Hubin, J. M. McCormick, N. W. Alcock, H. J. Clase and D. H. Busch, *Inorganic Chemistry*, 1999, **38**, 4435-4446.
14. T. J. Hubin, N. W. Alcock and D. Busch, H., *Acta Cryst*, 1999, **C55**, 1404-1406.
15. T. J. Hubin, N. W. Alcock and D. H. Busch, *Acta Crystallographica Section C-Crystal Structure Communications*, 2000, **56**, 37-39.
16. T. J. Hubin, N. W. Alcock, H. J. Clase and D. H. Busch, *Acta Crystallographica Section C-Crystal Structure Communications*, 1999, **55**, 1402-1404.
17. S. R. Collinson, N. W. Alcock, T. J. Hubin and D. H. Busch, *Journal of Coordination Chemistry*, 2001, **52**, 317-331.
18. T. J. Hubin, N. W. Alcock, H. J. Clase and D. H. Busch, *Supramolecular Chemistry*, 2001, **13**, 261-276.
19. A. Khan, G. Nicholson, J. Greenman, L. Madden, G. McRobbie, C. Pannecouque, E. De Clercq, J. D. Silversides, R. Ullom, D. L. Maples, R. D. Maples, T. J. Hubin and S. J. Archibald, *J. Am. Chem. Soc.*, 2009, **131**, 3416-3417.
20. A. Khan, G. Nicholson, G. McRobbie, J. Greenman, C. Pannecouque, D. Daelemans, D. Schols, E. De Clercq, T. J. Hubin and S. J. Archibald, *Antiviral Research*, 2009, **82**, DOI 10.1016/j.antiviral.2009.1002.1141|1136.
21. J. C. Timmons and T. J. Hubin, *Coordination Chemistry Reviews*, 2010, **254**, 1661-1685.
22. R. Smith, D. Huskens, D. Daelemans, R. E. Mewis, C. D. Garcia, A. N. Cain, T. N. C. Freeman, C. Pannecouque, E.

De Clercq, D. Schols, T. J. Hubin and S. J. Archibald, *Dalton Transactions*, 2012, **41**, 11369-11377.
23. P. N. A. Amoyaw, K. Pham, A. N. Cain, J. M. McClain, T. J. Hubin and M. O. F. Khan, *Current Organic Synthesis*, 2014, **11**, 916-921.
24. J. Panneerselvam, J. K. Jin, M. Shanker, J. Lauderdale, J. Bates, Q. Wang, Y. D. Zhao, S. J. Archibald, T. J. Hubin and R. Ramesh, *Plos One*, 2015, **10**.
25. M. O. F. Khan, J. Keiser, P. N. A. Amoyay, M. F. Hossain, M. Vargas, J. G. Le, N. C. Simpson, R. K. D., T. N. Carder Freeman, T. R. Hasley, R. D. Maples, S. J. Archibald and T. J. Hubin, *Antimicr. Agents Chemoth.*, 2016, **60**, 5331-5336.
26. R. D. Maples, A. N. Cain, B. P. Burke, J. D. Silversides, R. Mewis, T. D'huys, D. Schols, D. P. Linder, S. J. Archibald and T. J. Hubin, *Chemistry: A European Journal*, 2016, **22**, 12916-12930.
27. A. N. Cain, C. F. T. N., K. D. Roewe, D. L. Cockriel, T. R. Hasley, R. D. Maples, E. M. A. Allbritton, T. D'Huys, T. van Loy, B. P. Burke, T. J. Prior, D. Schols, S. J. Archibald and T. J. Hubin, *Dalton Transactions*, 2019, **48**, 2785-2801.
28. C. S. M. Benjamin P. Burke, Rhiannon E. Lee, Isaline Renard, Shubhanchi, G. S. C. Nigam, Thomas D'Huys, Torsten Ruest, Juozas Domarkas, James A. Thompson, Timothy J. Hubin, Dominique Schols, Christopher J. Cawthorne, Stephen J. and Archibald, *Journal of Nuclear Medicine*, 2020, **61**, 123-128.
29. G. C. Valks, G. McRobbie, E. A. Lewis, T. J. Hubin, T. M. Hunter, P. J. Sadler, C. Pannecouque, E. De Clercq and S. J. Archibald, *Journal of Medicinal Chemistry*, 2006, **49**, 6162-6165.
30. T. J. Hubin, J. M. McCormick, S. R. Collinson, M. Buchalova, C. M. Perkins, N. W. Alcock, P. K. Kahol, A. Raghunathan and D. H. Busch, *Journal of the American Chemical Society*, 2000, **122**, 2512-2522.
31. *US Pat.,* 6,218,351, 2001.
32. T. J. Hubin, J. M. McCormick, N. W. Alcock and D. H. Busch, *Inorganic Chemistry*, 2001, **40**, 435-444.
33. T. J. Hubin, N. W. Alcock, H. J. Clase, L. L. Seib and D. H. Busch, *Inorganica Chimica Acta*, 2002, **337**, 91-102.
34. T. J. Hubin, J. M. McCormick, S. R. Collinson, N. W. Alcock, H. J. Clase and D. H. Busch, *Inorganica Chimica Acta*, 2003, **346**, 76-86.
35. T. J. Hubin, N. W. Alcock, M. D. Morton and D. H. Busch, *Inorganica Chimica Acta*, 2003, **348**, 33-40.
36. *US Pat.,* 6,906,189, 2005.
37. D. H. Busch, *Accounts Chem Res*, **1978**, ***11*** 392-400.
38. A. D. Shircliff, K. R. Wilson, D. J. Smith, D. G. Jones and T. J. Hubin, *Abstracts of Papers of the American Chemical Society*, 2014, **247**.
39. Z. Zhang, K. L. Coats, Z. Q. Chen, T. J. Hubin and G. C. Yin, *Inorganic Chemistry*, 2014, **53**, 11937-11947.
40. D. G. Jones, K. R. Wilson, D. J. Cannon-Smith, A. D. Shircliff, Z. Zhang, Z. Q. Chen, T. J. Prior, G. C. Yin and T. J. Hubin, *Inorganic Chemistry*, 2015, **54**, 2221-2234.
41. D. L. Matz, D. G. Jones, K. D. Roewe, M. J. Gorbet, Z. Zhang, Z. Q. Chen, T. J. Prior, S. J. Archibald, G. C. Yin and T. J. Hubin, *Dalton Transactions*, 2015, **44**, 12210-12224.
42. K. R. Wilson, D. J. Cannon-Smith, B. P. Burke, O. C. Birdsong, S. J. Archibald and T. J. Hubin, *Polyhedron*, 2016, **114**, 118-127.
43. S. M. Brewer, K. R. Wilson, D. G. Jones, E. W. Reinheimer, S. J. Archibald, T. J. Prior, M. A. Ayala, A. L. Foster, T. J. Hubin and K. N. Green, *Inorg. Chem.*, 2018, **57**, 8890-8902.
44. A. D. Shircliff, B. P. Burke, D. J. Davilla, Burgess, G. E., F. A. Okorocha, A. Shrestha, E. M. A. Allbritton, P. T. Nguyen, Lamar, R. L., D. G. Jones, M.-J. Gorbet, M. B. Allen, J. I. Eze, A. T. Fernandez, Ramirez, D., S. J. Archibald, T. J. Prior, J. A. Krause, A. G. Oliver and T. J. Hubin, *Chem. Commun.*, 2020, **56**, 7519-7522.
45. J. E. Richman and T. J. Atkins, *J. Am. Chem. Soc.*, 1974, **96**, 2268-2270.
46. T. J. Atkins , J. E. Richman and a. W. F. Oettle, *Org. Synth.*, **1978**, ***58***, 86-95.
47. P. Osvath, N. F. Curtis and D. C. Weatherburn, *Aust. J. Chem.*, 1987, **40**, 347-360.
48. Z. Kovacs, E. A. Archer, M. K. Russell and A. D. Sherry, *Synthetic Communications*, 1999, **29**, 2817-2822.
49. H. D. Beibei Shao, Xinyu Hao, Rongwen Lu, Yi Luo, Shufen Zhang, *Journal*, 2016, **24**, 1000-1006.
50. D. P. Riley and R. H. Weiss, *Journal of the American Chemical Society*, 1994, **116**, 387-388.
51. Dennis P. Riley, Patrick J. Lennon, a. William L. Neumann and R. H. Weiss, *Journal of the American Chemical Society*, 1997, **119**, 6522-6528.
52. X.-Q. Wei, K. Qian, H.-Y. Wei and X.-Y. Wang, 2016, DOI: 10.1021/acs.inorgchem.6b00787.
53. P. Osvath, D. C. Weatherburn and W. T. Robinson, *Transition Metal Chemistry*, 1991, **16**, 344-347.
54. K. Sakai, Y. Yamada and T. Tsubomura, *Inorg Chem*, 1996, **35**, 3163-3172.
55. Daike and X. G. Li, Minyu Tan, Xin Wang, *Polyhedron*, 1997, **16**, 3941-4189.
56. S.-S. Ting-Hai Yang and K. Z. Bao, Yi-Zhi Li, Li-Min Zheng, *Wuji Huaxue Xuebao*, 2008, **24**, 937.
57. W.-J. L. a. C.-S. C. T.-H. Lu, *Acta Crystallographica Section C*, 1993, **C49**, 961-963.
58. A. W. Addison, T. N. Rao, J. Reedijk, J. v. Rijn and G. C. Verschoor, *Journal of the Chemical Society, Dalton Transactions*, 1984, DOI: 10.1039/DT9840001349.
59. H. G. Johannes Notni, Ernst Anders, *European Journal of Inorganic Chemistry*, 2006, DOI: 10.1002/ejic.200500947, 1444.
60. Y.-J. Chen, P. Xie, M. J. Heeg and J. F. Endicott, *Inorg Chem*, 2006, **45**, 6282-6297.
61. G.-H. Ning, Y. Inokuma and M. Fujita, *Chemistry - An Asian Journal*, 2013, **8**, 2596-2599.
62. E. K. Barefield and D. H. Busch, *Inorg Chem*, 1971, **10**, 108-114.
63. V. L. Goedken and D. H. Busch, *Inorg Chem*, 1971, **10**, 2679-2682.
64. J. C. Dabrowiak, F. V. Lovecchio, V. L. Goedken and D. H. Busch, *Journal of the American Chemical Society*, 1972, **94**, 5502-5504.
65. D. F. Mahoney and J. K. Beattie, *Inorg Chem*, 1973, **12**, 2561-2565.
66. S. E. Diamond, G. M. Tom and H. Taube, *J. Am. Chem. Soc.*, 1975, **97**, 2661-2664.
67. P. K. Chan, D. A. Isabirye and C. K. Poon, *Inorg Chem*, 1975, **14**, 2579-2580.
68. D. D. Walker and H. Taube, *Inorg Chem*, 1981, **20**, 2828-2834.
69. C. M. Che, S. S. Kwong, C. K. Poon, T. F. Lai and T. C. W. Mak, *Inorg Chem*, 1985, **24**, 1359-1363.

70. C. K. Poon and C. M. Che, *Inorg Chem*, 1981, **20**, 1640-1643.
71. K. Q. Ferreira, A. M. Lucchesi, Z. N. da Rocha and R. S. da Silva, *Inorganica Chimica Acta*, 2002, **328**, 147-151.
72. K. Q. Ferreira, F. G. Santos, Z. N. da Rocha, T. Guaratini, R. S. da Silva and E. Tfouni, *Inorganic Chemistry Communications*, 2004, **7**, 204-208.
73. K. Q. Ferreira, L. N. Cardoso, S. Nikolaou, Z. N. da Rocha, R. S. da Silva and E. Tfouni, *Inorg Chem*, 2005, **44**, 5544-5546.
74. A. B. P. Lever, *Inorganic Electronic Spectroscopy, 2nd ed*, Elsevier, Amsterdam, 1984.
75. *Journal*, 2014.
76. G. M. Sheldrick, *Journal*, 2014.
77. G. M. Sheldrick, *Acta Cryst A*, 2015, **71**, 3-8.